Flight simulation testing of a turbulence model based on a Synthetic Eddy Method

Sergio Henriquez Huecas
S.Henriquez-Huecas@liverpool.ac.uk
University of Liverpool
Liverpool, United Kingdom

Prof. Mark White
mdw@liverpool.ac.uk
University of Liverpool
Liverpool, United Kingdom

Prof. George Barakos
George.Barakos@glasgow.ac.uk
University of Glasgow
Glasgow, United Kingdom

Abstract

This paper presents initial analysis of an ongoing series of flight simulation trials of a new turbulence model based on a synthetic eddy method (SEM). The model is based on the generation of a random distribution of turbulence generating Eddies within a control model surrounding the aircraft. Eddies are displaced by the flow and regenerated at the inflow as they leave the simulation domain. The model allows adjustment of turbulence intensity by adjusting the value of Reynolds stress tensor and of frequency spectra through adjustment of eddy sizes, allowing for a more realistic representation of broadband turbulence. Compared to other random turbulence models, preserving the location of the Eddies in the control volume ensures automatically that turbulence across different aircraft locations is automatically correlated.

Piloted flight simulation tests show that both, levels of turbulence intensity and frequency of the induced turbulence have a strong effect on workload and task performance. Increases in turbulence intensity result in a direct increase in pilot workload and reduced task performance. However changes in frequency of turbulence present a more complex picture dependent on flight condition and aircraft response.

Notation

Nomenclature

$\boldsymbol{A}$; A_{ij}	Cholesky decomposition of Reynolds Stresses
$f_\sigma(\boldsymbol{x}-\boldsymbol{x}^k)$	Three-dimensional Eddy shape function
$f(x)$	One dimensional Eddy shape function
N	Number of Eddies
$\boldsymbol{r}$	Distance vector
Re_{ij}	Reynolds Stress Tensor
$\boldsymbol{u'} = [u'_x, u'_y, u'_z]$	Turbulence velocity
V_{flow}	Flow velocity
ε_j^k	Sign of velocity generated by Eddy k along axis i
$\boldsymbol{\sigma} = [\sigma_x, \sigma_y, \sigma_z]$	Eddy size
ϕ_{ij}	Power spectral density between axis i and j components
$\boldsymbol{\omega}$	frequency

Abbreviations

ACP	Aerodynamic Computation point
BWR	Bedford workload rating
MTE	Mission task element
PH	Precision Hover
PIO	Pilot Induced Oscillations
PSD	Power Spectral Density
RCAH	Rate Command Attitude Hold
RMS	Root Mean Square
SCAS	Stability Control Augmentation System
SEM	Synthetic Eddy Method
S&L	Steady and level flight

Introduction

NITROS (Network for Innovative Training on ROtorcraft Safety) [1] is a European Joint Action Project, conducted as part of the Marie Sklowdoska Curie program. It consists of twelve double doctorate projects at four leading European universities in the field of aerospace engineering (Politecnico Di Milano, Technical University of Delft, University of Glasgow and University of Liverpool) focused on research in the areas of rotorcraft modelling and design, pilot training and human-machine interface and environment – rotorcraft interaction with the aim of enhancing rotorcraft safety.

This project conducted jointly by the Universities of Liverpool and Glasgow focusses on addressing the interactions between helicopter, pilot and the surrounding aerodynamic environment. Helicopters are used in a wide variety of roles, such as shipborne [2] and offshore missions [3] during which they can be subjected to a large range of environmental hazards where the risk of an accidental encounter with an airwake could affect flight safety. An increasingly relevant area is the issue of hazards resulting from encounters with wind turbine airwakes [4]. Initial results from testing conducted for the GARTEUR HC/AG-23 [5] Action Group shows that further research is needed to adequately understand how the combination of environment and aircraft handling qualities influence the outcome of an accidental wake encounter.

However, as of now, a unified approach to the assessment and mitigation of hazards resulting from rotorcraft operations in turbulence or accidental airwake encounters is still lacking. EASA certifications for small (CS – 27, [6]) and large (CS – 29, [7]) rotorcraft only establish the need to ensure controllability and structural resistance under expected gust conditions. ADS – 33 [8] offers maybe the most comprehensive criteria to asses aircraft and stability augmentation system response to upsets. Although the focus is largely on single external upsets and esponse criteria to continuous turbulence has been adapted from the control bandwidth criteria. There seems to be little supporting data for this [9] and it is intended to be replaced by a disturbance response bandwidth criteria in the future [10]. The UK Civil Aviation Authority (CAA) establishes a maximum standard deviation of vertical wind velocity over landing areas on offshore platforms to allow operations [11]. These limits were defined after a series of piloted and offline flight simulation studies using airwake data collected from wind tunnel tests [3] [12].

Such lack of unified criteria might partly be because adequately modelling the interaction between a rotorcraft and its surrounding aerodynamic environment in real-time for piloted simulation has proved to be a challenging endeavour. The current state of the art is the use of stored time accurate airwake solutions which have been pre-computed using Computational Fluid Dynamics (CFD) tools and are accessed during simulated flight [2]. However, computational costs and storage requirements means that only a limited number of short duration airwake solutions will usually be available. To address some of these issues, stochastic turbulence models [13] can generate random, low intensity, high frequency turbulent flow in real time superimposed over lower fidelity airwake solutions.

Helicopter turbulence models are usually built around the implementation of Von Karman's formula [14] or Dryden models [15] based on the assumption of a homogeneous, isotropic and frozen turbulence field that approaches towards the aircraft with its aerodynamic velocity [16]. However adaptation to the broad range of flight conditions and the inclusion of rotation effects when computing turbulence correlation between the different blade elements is necessary [17], [18]. A simpler approach was suggested by McFarland et al. in [19], by distributing a turbulent velocity field over the rotor plane across a number of stations and displacing it by one station at each time step. A three dimensional extension to this method was proposed by Ji et al. in [20]. This method however has limitations when flight or environmental conditions experience large changes within a small number of time steps. Finally Lusardi et al. [21] and Seher-Weiss et al. [22] describe the use of System Identification techniques from flight test measurements for modelling turbulence upsets as equivalent control inputs. These models however depend on the availability flight test data from a specific combination of aircraft, environmental conditions and flight task. Adaptations to similar conditions are possible, Hess suggest in [23] a scaling technique to adapt the model to similar helicopters of differing rotor size and speed. A further

improvement is presented by Wajih et al. in [24], where the turbulence inputs resulting from turbulence over a ships flight deck are adapted according to differing levels of intensity along the flight path.

Implementation of Synthetic Eddy Turbulence

SEM theory and coupling with FlightLab

The turbulence model presented in this paper is proposed as a first step to solve some of these issues. It is based on a Synthetic Eddy Model (SEM) first proposed by Jarrin [25] to generate realistic turbulence oscillations at the inflow of CFD simulations. A brief description of the basics is presented here. The detailed description, implementation and verification of the model is given in Ref [26].

A box–shaped control volume is defined around the aircraft and completely filled by a random uniform distribution of N eddies, an inflow is defined facing towards the direction of the incoming aerodynamic velocity (see Figure 1).

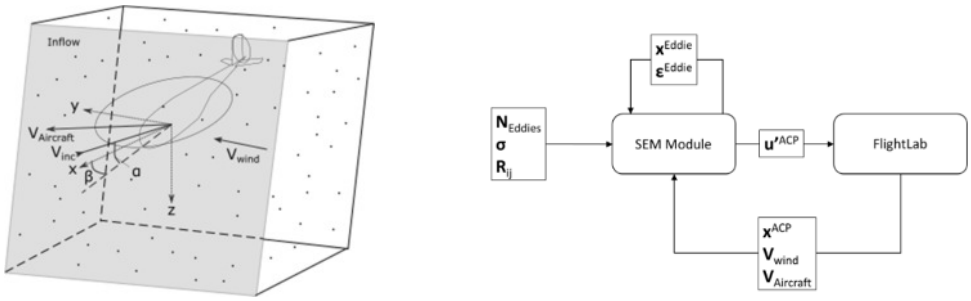

Figure 1: Left: Diagram of the control volume used for the synthetic eddy method. Right: Flow chart of data exchanged between the SEM module and FLIGHTLAB.

On each time step an eddy located on $\boldsymbol{x}^k$ generates a turbulent velocity perturbation on an ACP located at $\boldsymbol{x}^{\boldsymbol{ACP}}$**.** The total induced turbulence on each ACP is obtained by adding the contribution of each eddy:

$$u'^{ACP}_i = \frac{1}{\sqrt{N}} \sum_{k=1}^{N_{Eddies}} A_{ij} \varepsilon_j^k f_\sigma(\boldsymbol{x}^{ACP} - \boldsymbol{x}^k) \quad (1)$$

Where ε_j^k is a randomly assigned sign and $\boldsymbol{A}$ is the Cholesky decomposition of the Reynolds stress tensor ($Re_{ij} = \langle u'_i u'_j \rangle$), which controls the resulting turbulence intensity:

$$\boldsymbol{A} = \begin{bmatrix} \sqrt{Re_{11}} & 0 & 0 \\ \frac{Re_{21}}{A_{11}} & \sqrt{Re_{22} - A_{21}^2} & 0 \\ \frac{Re_{31}}{A_{11}} & \frac{Re_{32} - A_{21}A_{31}}{A_{22}} & \sqrt{Re_{33} - A_{31}^2 - A_{32}^2} \end{bmatrix} \quad (2)$$

The shape function $f_{\sigma(\boldsymbol{x})}(\boldsymbol{x} - \boldsymbol{x}^k)$ relates the shape and size of the eddies, σ_i, with the decay of their effect with distance.

$$f_{\sigma(x)}(\boldsymbol{x} - \boldsymbol{x}^k) = \sqrt{\frac{V_B}{\sigma^3}} * f\left(\frac{x - x^k}{\sigma_x}\right) * f\left(\frac{y - y^k}{\sigma_y}\right) f\left(\frac{z - z^k}{\sigma_z}\right) \quad (3)$$

Each component of the shape function needs to fulfil the normalization condition:

$$\int_{-\infty}^{+\infty} f^2(x) = \int_{-\sigma}^{+\sigma} f^2(x) = 1 \quad (4)$$

After each time step, the population of eddies is displaced with the wind velocity resulting in a random frozen turbulence field which displaces itself with ambient wind velocity. Eddies falling outside the control volume at the start of the time step are regenerated at a random location at the inflow.

The frequency spectra of the resulting turbulence are given by:

5 $$\phi_{ij}(\boldsymbol{x}, \boldsymbol{\omega}) = Re_{ij} \frac{\sigma}{|\bar{\boldsymbol{u}}|} \left| \mathcal{F}_{\frac{\sigma\omega}{|\bar{u}|}}\{f\} \right|^2$$

Where $\mathcal{F}_{\frac{\sigma\omega}{|\bar{u}|}}\{f\}$ is the fourier transform of function *f* at a frequency scaled by $\frac{\sigma\omega}{|\bar{u}|}$. The turbulence spectra can be adjusted by altering the value of Reynolds stress tensor, eddy size and shape function. Figure 3 a) shows the effect of changes in the value of Re_{ij} which determines the resulting standard deviation in turbulent velocities generated for each axis. And for a control volume completely filled with a uniform distribution of eddies, the value of average frequency is proportional to the ratio between incident flow velocity and characteristic eddy length, $\frac{V_{flow}}{\sigma}$, as shown in Figure 3 b). For adjustment of the SEM generated turbulence, values for these parameters can be obtained from measurements or CFD simulations [27], [28].

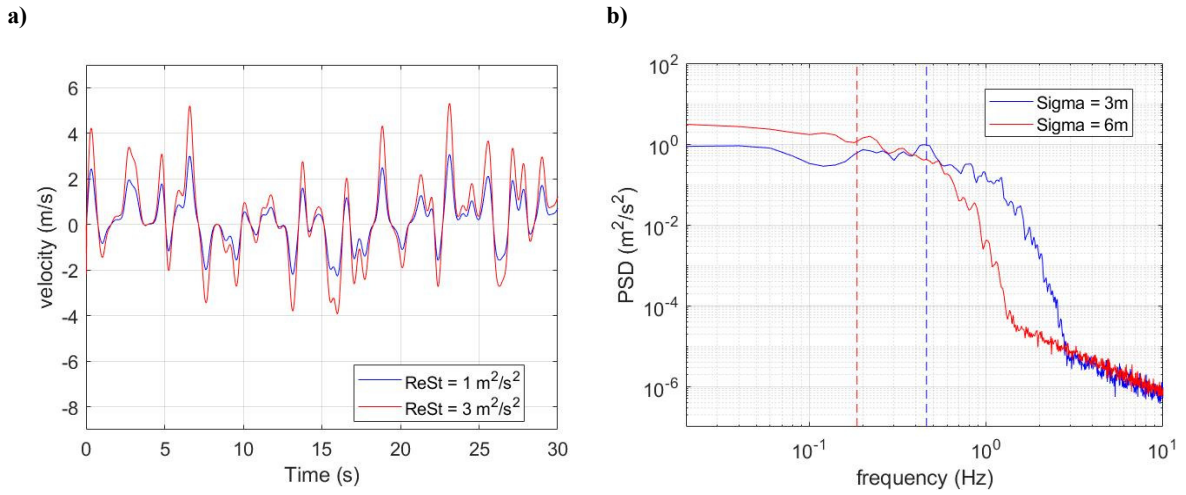

Figure 2: Effect of SEM parameters on generated turbulence: a) changes in value of Reynolds Stresses, b) changes in eddy size. Vertical dashed lines indicate average frequencies. All graphs correspond to vertical turbulent velocity at a fixed point under a 10 kts wind.

Two different shape functions have been implemented and tested. Initial validation and testing were conducted using a tent shape function:

6 $$f(x) = \begin{cases} \sqrt{\frac{3}{2}} * (1 - |x|), & if\ |x| < 1 \\ 0, & if\ |x| > 1 \end{cases}$$

More recent testing, including simulation test described in this article, has been conducted using a Gaussian shaped function:

7 $$f(x) = \begin{cases} C * e^{-k*x^2}, & if\ |x| < 1 \\ 0, & if\ |x| > 1 \end{cases}$$

Where the value of C is chosen to comply with the normalization condition:

8 $$C^2 = \frac{\sqrt{2 * k}}{\sqrt{\pi} * \int_{-\sqrt{2k}}^{\sqrt{2k}} e^{-x^2}\, dx}$$

A comparison of the turbulence generated using different shape functions is presented in Figure 3. Compared to a tent shaped eddy, a Gaussian shape function with a value of $k = 4.5$ shows a shift in the fall of power density towards higher frequencies and a reduction at lower frequencies. Another effect is a reduction in the appearance of low intensity high frequency peaks. These effects increase for a value of $k = 9$. This reduction in high frequency noise should allow for an easier adjustment of the

turbulence spectra using a multi scale eddy adaptation in the future [29], [30]. For this reason, flight simulation testing presented in this paper has been performed using the gaussian shape function.

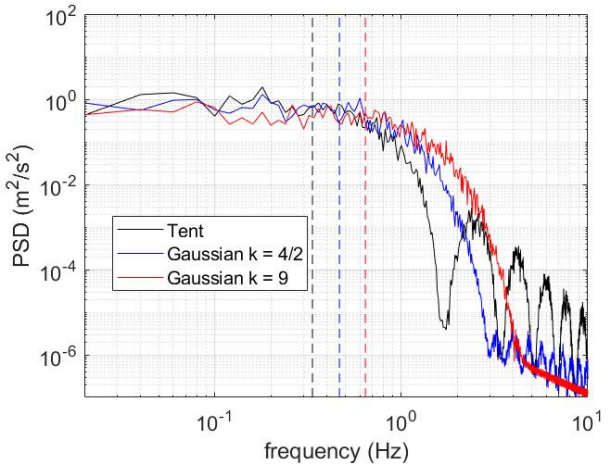

Figure 3: Effect of changes in shape function. Vertical dashed lines indicate average frequencies. All graphs correspond to vertical turbulent velocity at a fixed point under a 20 kts wind.

The main advantage of SEM compared to previous turbulence models is that the location of the eddies near the aircraft is preserved for each time step. This ensures that turbulence induced for each ACP is coherent with the effects on the rest of the aircraft even if aircraft flight velocities experience large changes in a small number of time steps, this is shown in Figure 4 a) where the vertical turbulent flow at the aerodynamic computation points at the fuselage and root and tip of one rotor blade. Figure 4 b) shows the same vertical turbulence velocity at the tip of opposite blades.

a) **b)**

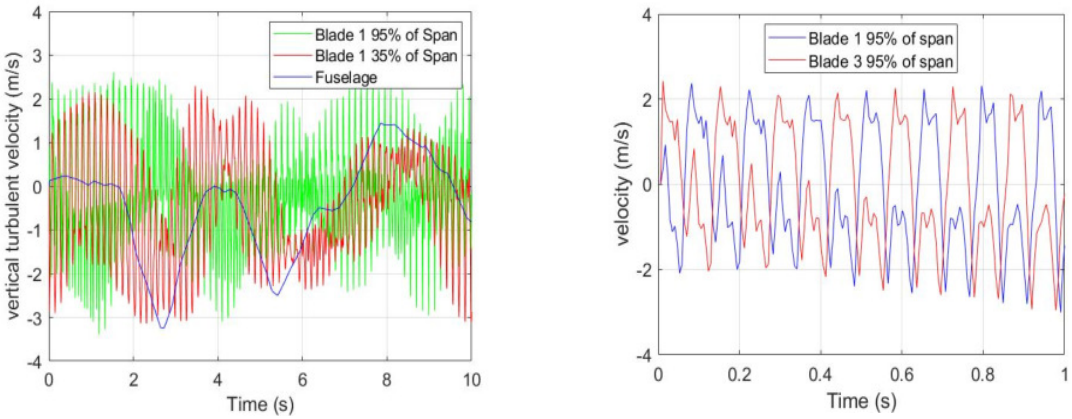

Figure 4: Correlation between turbulence induced vertical flow velocities in hover under a 10kts, 90deg green wind: a) At fuselage, blade root and blade tip. c) At the tip of opposite blades.

Offline simulations

The SEM turbulence model has been coupled with FLIGHTLAB [31] helicopter models developed at the University of Liverpool. Initial analysis and flight simulation testing were performed using a Bo105 helicopter model [32], [33] with results suggesting that handling qualities deficiencies, especially lack of a stability augmentation system and strong interaxis couplings, made it difficult to discern the effect of turbulence on handling.

For this reason a Bell-412 model [34], based on the Advanced Systems Research Aircraft (ASRA) operated by the Canadian National Research Council (NRC) [35], was integrated with the SEM model. This aircraft is equipped with a stability augmentation system in roll, pitch and yaw axis and presents improved handling qualities allowing for better identification of their deterioration with turbulence.

Figure 5 shows turbulence induced moments in a) roll, b) pitch and c) yaw as well as d) oscillations in aircraft thrust coefficient with the stability system turned off and aircraft movement in all axis frozen as well as with the stability system configured as rate command attitude hold (RCAH) and only the vertical axis frozen in order to prevent any collision with the ground. Turbulence effects in rotor thrust and moments are clearly appreciable within the 0.1 – 1Hz frequency range that affects aircraft and pilot handling [36]. Impact of turbulence decays rapidly at higher frequencies but extends across the whole frequency spectrum with reduced peaks at multiples of four times the rotor frequency. It can be seen that the SCAS system is capable of counteracting turbulence induced moments in the low frequency (below 0.5Hz) domain for all three axis, especially in the longitudinal and lateral axis, resulting in an overall decrease in the amplitude of induced disturbances. Above 0.5Hz this reduction becomes less noticeable, resulting in an overall shift of disturbances towards higher frequencies and the appearance of peaks in roll and pitch disturbances at around 1Hz and 0.5Hz. These frequencies are near to the Bell 412 longitudinal and lateral control bandwidth limits in attitude command and attitude hold configuration [34]. The Bell 412 lacks any stability augmentation in the heave axis, and Figure 5 d) shows that engaging the stability system does not result in any alleviation of oscillations in thrust.

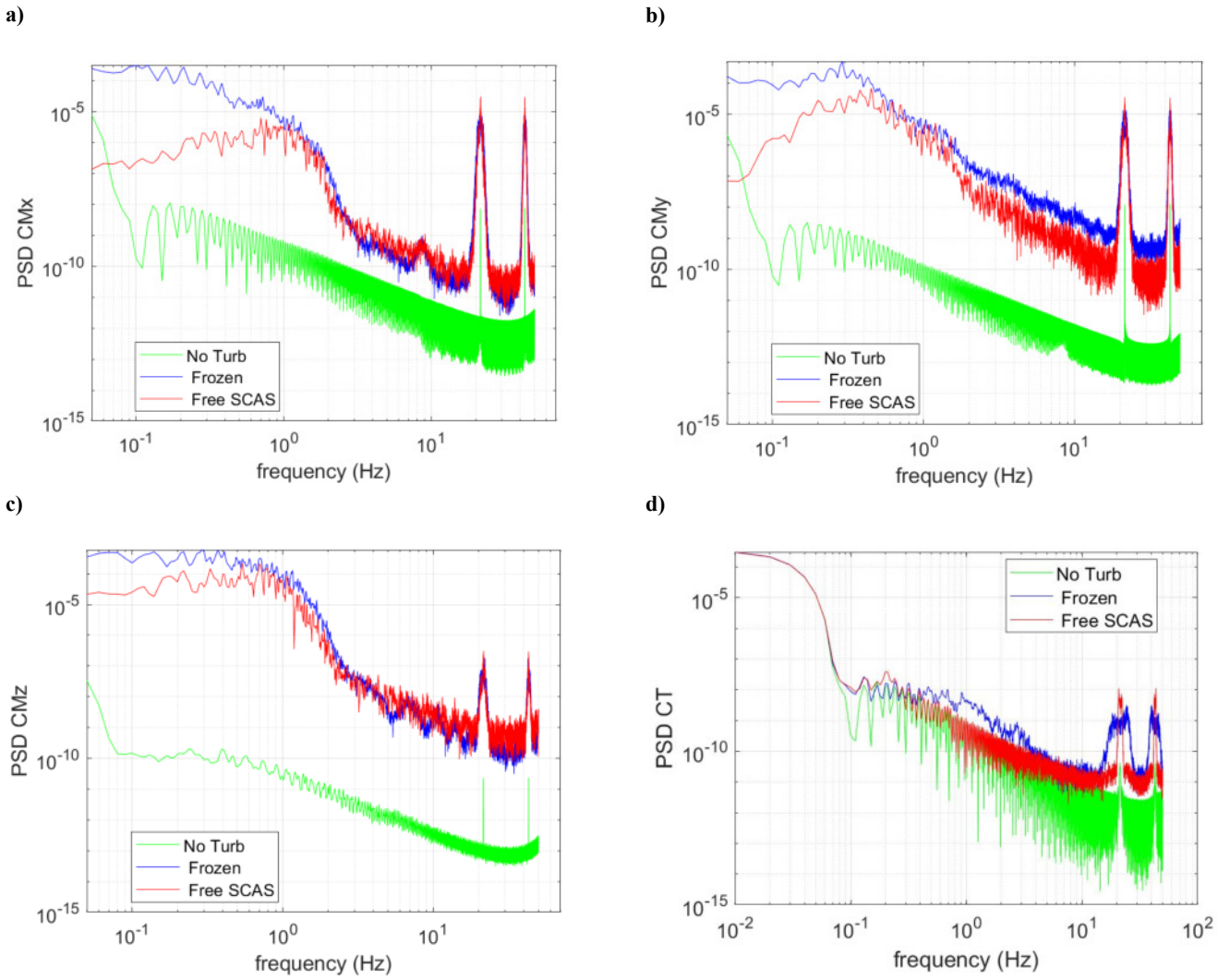

Figure 5: Comparison of turbulence induced disturbances with and without stability augmentation: a), b) and c) aircraft moment coefficients in roll pitch and yaw respectively d) main rotor thrust coefficient. Cases include: hover without turbulence, frozen aircraft under turbulence, unfrozen aircraft with stability system activated and configured as RCAH. Turbulence parameters are: Re_{ii} = 1 m^2/s^2, σ_i = 3m, wind of 10kts, 90 deg green.

Figure 6 shows the effect of differences in Reynolds stress and eddy size in turbulence induced moments in a) roll, b) pitch and c) yaw. Changes in the value of Re_{ii}, change the amplitude of induced disturbances but keep the overall shape of the disturbance spectra. Increasing eddy size, decreases

the frequency at which induced disturbances reach their peak, resulting in lower average frequencies for induced disturbances which the SCAS system seem more capable of counteracting.

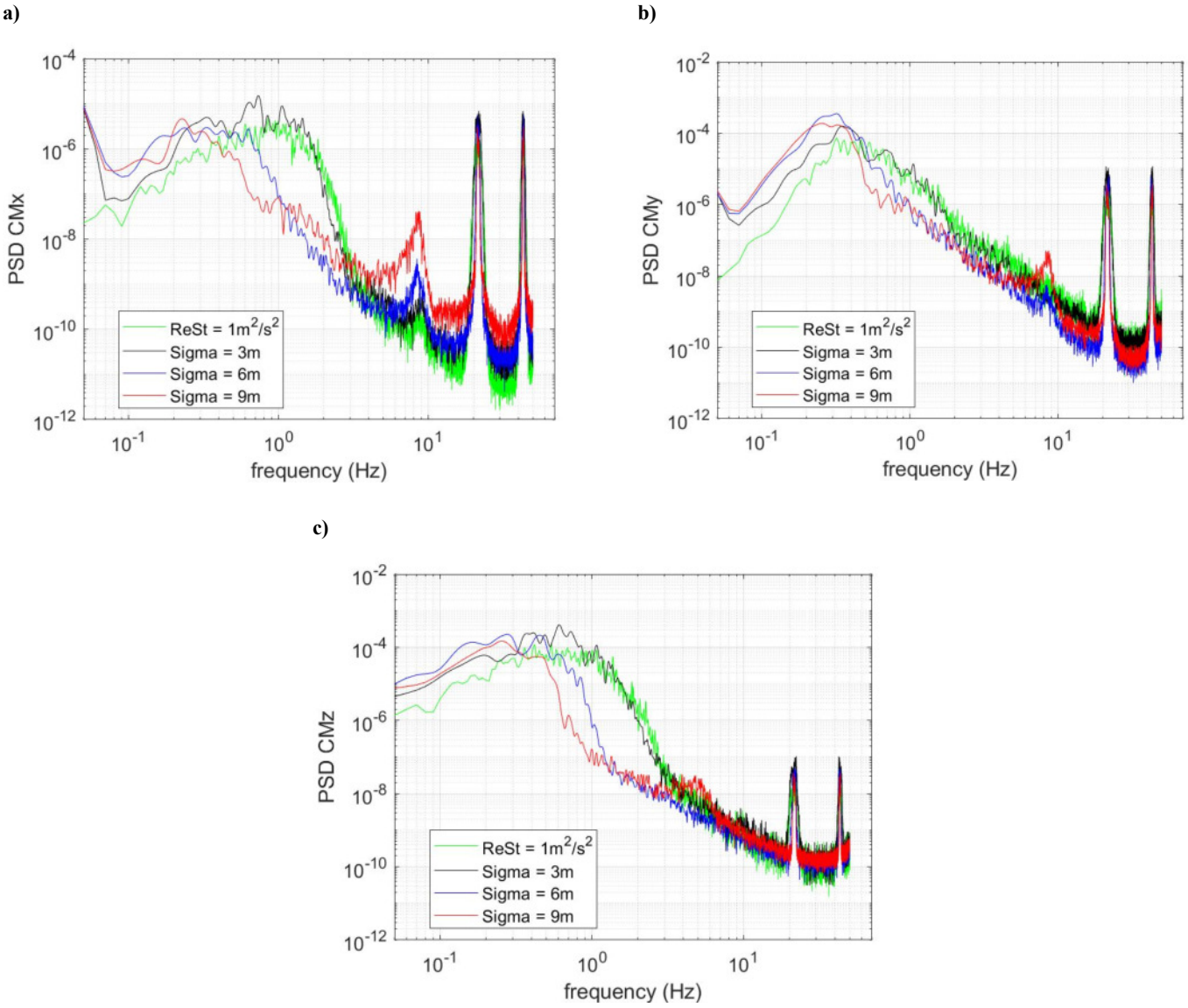

Figure 6: turbulence induced moments in a) roll, b) pitch, c) yaw under turbulence conditions of: Re_{ii} = 1 m^2/s^2, σ_i = 3m, Re_{ii} = 3 m^2/s^2, σ_i = 3m, Re_{ii} = 3 m^2/s^2, σ_i = 6m, Re_{ii} = 3 m^2/s^2, σ_i = 9m. Wind of 10kts, 90 deg green.

Flight simulation feasibility tests – Bo105

During development of the SEM model, flight simulation testing was performed in order to assess the real time capabilities of the model and obtain an initial estimation of induced turbulence on aircraft handling and pilot workload. The test was conducted at the University of Liverpool's HELIFLIGHT – R flight simulator [37] using the FLIGHTLAB Bo105 model i.e. with no SCAS. Tests were conducted without using the motion platform. A complete discussion of these preliminary tests is provided in [30] with the most relevant results summarized here.

The pilot was instructed to attempt two tasks, both inspired by maneuvers that might be common during operations to offshore wind farms: the position keeping segment of the ADS - 33 precision hover (PH) mission task element (MTE) and a straight and level (S&L) low speed (30kts) flight task. Workload ratings awarded, which can be seen in Figure 7, show that increases in turbulence intensity lead to increases in required task workload and reduced spare capacity, the effect was especially strong during the precision hover task and much milder for the steady and level flight task.

Lack of an aircraft stability system and strong inter-axis couplings of the Bo105 [38] contributed significantly to the difficulty of the task. Even without turbulence the pilot awarded a BWR of 5 for the precision hover MTE, indicating that considerable compensation was required to complete the task and, as Figure 8 shows, desired performance was never achieved. This made it difficult at times to discern between turbulence induced disturbances and aircraft off-axis response to the pilot inputs. This was the main reason that the SEM model was integrated with a Bell 412 FLIGHTLAB model for further testing.

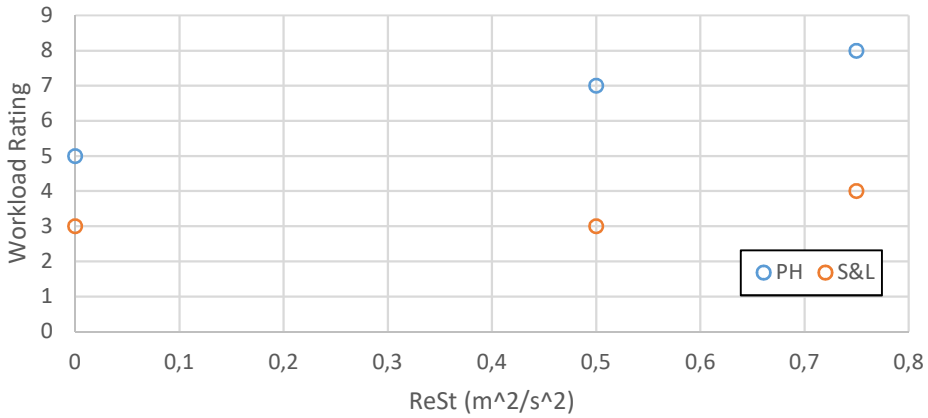

Figure 7: BWRs with increasing turbulence intensity

a) **b)**

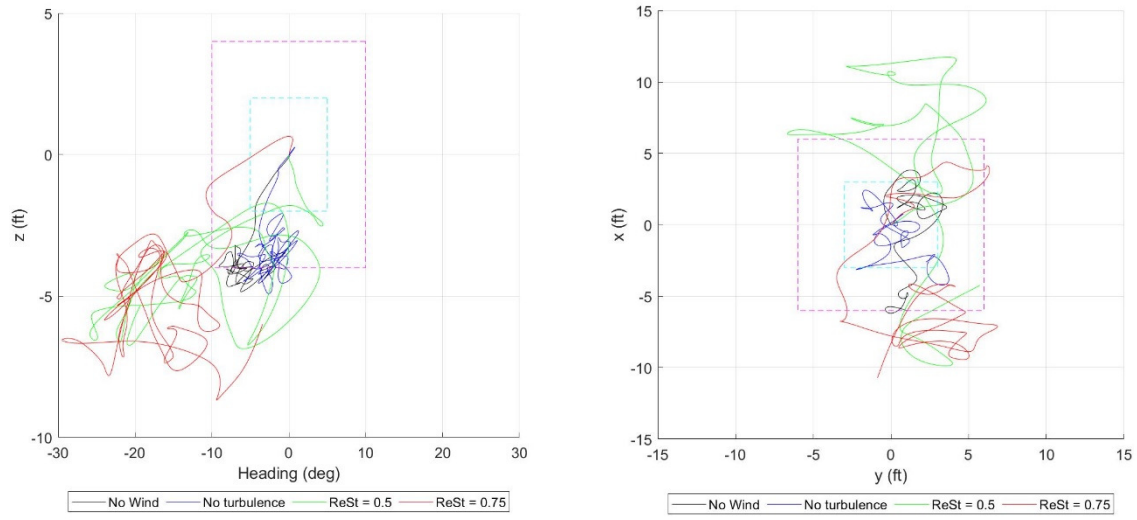

Figure 8: Performance of hover task. Deviations from start point: a) Heading and altitude. b) Lateral and longitudinal displacements. Dashed lines in cyan and magenta indicate boundaries for adequate and desired deviations respectively.

Finally, as shown in Figure 9, a trend was identified of increasing turbulence intensities leading to increasing values in the root mean square (RMS) of oscillations in aircraft moments (Figure 9 a) and forces (Figure 9 a and b) and required pilot response (Figure 9 c). The RMS is defined as the root square of power spectral density between the frequencies of 0.1Hz and 2Hz and has been positively correlated with pilot workload during flight simulation trials of shipboard landings [39] [40].

a)

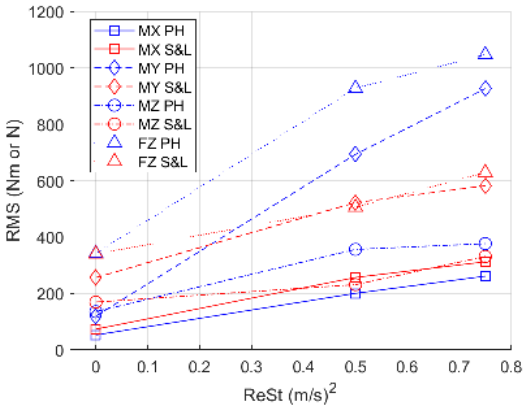

b)

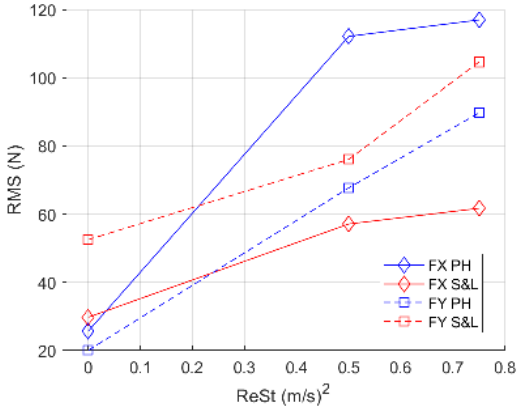

c)

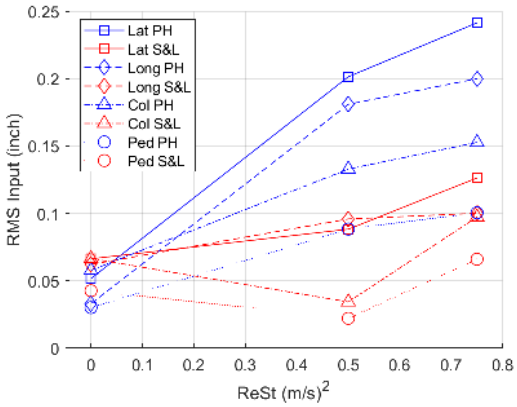

Figure 9: a) RMS of aircraft moments and vertical forces, b) RMS of aircraft longitudinal and lateral forces, c) RMS of pilot control inputs.

Ongoing flight simulation testing campaign – Bell412

The previously obtained results reported in this paper have shown that real time flight simulation is feasible with the current implementation of SEM based turbulence model. Testing has also pointed towards a possible relation between turbulence intensity, aircraft response parameters and pilot workload. However, the limited number data points and the deficient handling qualities of the Bo105 model means that those findings require validation through a more robust series of testing.

A flight simulation testing campaign is currently ongoing, using a FLIGHTLAB model of a Bell412 helicopter in order to test those findings and study the effect of changes in additional turbulence parameters. Improved handling qualities of the aircraft should make it easier to discern the effects of the turbulence and provide data of a better quality.

Objectives and method

Piloted flight simulation testing is being focused on hover and low speed flight conditions to assess how different adjustments of the SEM induced turbulence affect aircraft handling, pilot response and workload.

The objectives of the test were the following:

- Determine turbulence intensity limits suitable for flight simulation testing using the flight simulator motion platform.
- Determine turbulence intensity limits in which aircraft handling is still possible.
- Assess effects of different turbulence parameters on workload and handling during a low speed, low altitude precision task.
- Obtain subjective pilot opinion on the realism of the turbulence model.

The pilot performed a precision hover task as defined in ADS - 33 [8]. The aircraft started in hover at a distance to a target point oriented 45deg relative to the aircraft's heading and his task was defined as following:

Mission:

- Approach the target point and transition to hover over it in a single smooth manoeuvre and within the desired or adequate time limits.
- Once the hover has been captured, maintain aircraft position, altitude and heading within desired or adequate limits for at least 30s, or longer if the pilot deemed it necessary to provide an adequate evaluation.

A schematic of the task and test course is show in Figure 10. ADS – 33 desired and adequate requirements for cargo and utility helicopters, shown in Table 1, are used.

Parameter	Desired	Adequate
Attain stabilized hover over the target point before	5 sec	8 sec
Maintain horizontal position within:	3 ft	6 ft
Maintain vertical position within:	2 ft	4 ft
Maintain heading within:	5 deg	10 deg

Table 1: Desired and adequate limits for the precision hover task.

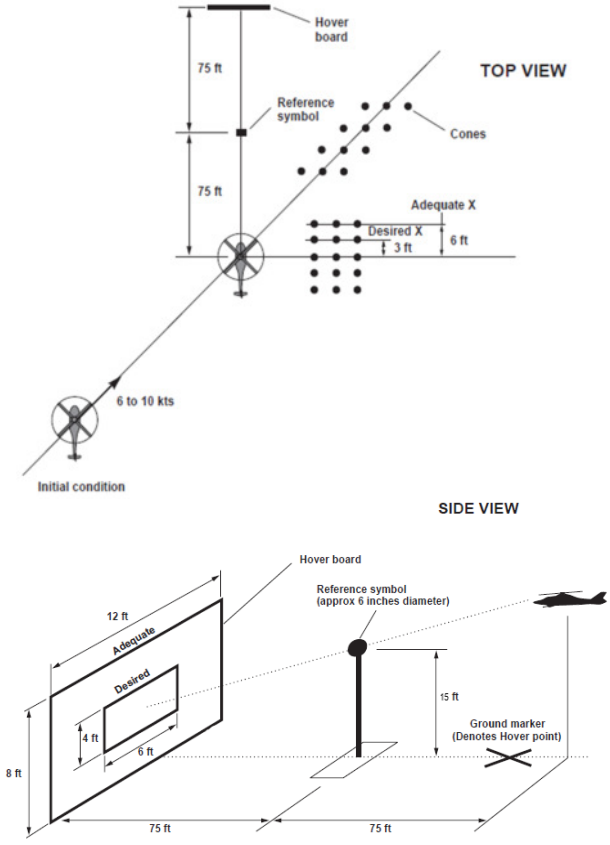

Figure 10: Schematic of Precision Hover test course and visual cues

The pilot was instructed to notify when he reached the hover point and when he had stabilized the aircraft in hover. The duration of the stabilization period was measured from the resulting audio recordings. Aircraft dynamics and pilot inputs have been recorded and the pilot awarded ratings based on the Bedford Workload (WL) [41] and Cooper Harper Handling Qualities rating (FHQ) scales [42] respectively, (see appendixes A and B). Additional pilot feedback and comments were also gathered during briefing, test and de-briefing.

Results

Runs performed and pilot ratings

All testing was performed under a 20kts, 90deg azimuth green wind. The wind speed is typical for wind turbine working conditions. The aircraft SCAS system was configured for RCAH in all cases. All runs were performed under isotropic, uniform turbulence conditions with turbulence intensity and eddy size equal for all three axes:

$$Re_{xx} = Re_{yy} = Re_{zz} = Re_{ii}$$
$$Re_{ij} = 0 \text{ for } i \neq j$$
$$\sigma_x = \sigma_y = \sigma_z = \sigma_i$$

The following turbulence parameters were changed for the different runs:

- **Turbulence intensity**: Modified by changing the values of Reynolds stresses uniformly in all directions. Starting from $R_{ii} = 0\ m^2/s^2$ values were gradually increased up to $R_{ii} = 6\ m^2/s^2$
- **Turbulence frequency:** Decreases by increasing eddie size uniformly in all directions. Starting at $\sigma_i = 3m$ and gradually increasing up to $\sigma_i = 9m$

The following table reports the performed runs, turbulence parameters and pilot ratings for each run:

Run		Re_{ii} (m^2/s^2)	σ_i (m)		Stabilization time (s)	FHQ Rating	WL rating		Comments
1		0	-		-	-	-		Free familiarization run
2		0	-		0	3	3		MTE without turbulence
3		1	3		0	-	-		Pilot asked for repeat
4		1	3		13	3	3		Repeat of 3
5		3	3		7	4	4		
6		3	6		0	5	6		
7		6	3		6	5	6		
8		3	9		4	6	7		

Table 2: Piloted simulation runs performed.

In the first run the pilot flew freely until he could familiarize himself with the flight simulator, controls and aircraft model. In the second run the pilot performed the task under a 20kts uniform wind but without any turbulence. The pilot awarded to this run workload and handling qualities ratings of 3, indicating some mild deficiencies in handling requiring minimal pilot compensation and allowing sufficient spare workload for additional tasks. According to his comments, roll and pitch control were the main drivers of workload when performing the task under conditions of no turbulence.

Effect of turbulence and increases in Reynolds Stress magnitude

The presence of turbulence results in handling deteriorations and workload increases which become larger under increasing levels of turbulence intensity. Flight handling qualities (FHQ) and workload ratings for different turbulence intensities are shown in Figure 11. All runs discussed in this chapter were done with the same eddy size of σ_i = 3m. The effects range from minimal for the lowest turbulence intensity tested, Re_{ii} = 1 (m^2/s^2), where the pilot awarded the same handling qualities and workload ratings of 3 as the case without turbulence, up to level 2 ratings of 5 in FHQ and 6 in WL, indicating a need for considerable pilot compensation and leaving little to no spare capacity for additional tasks.

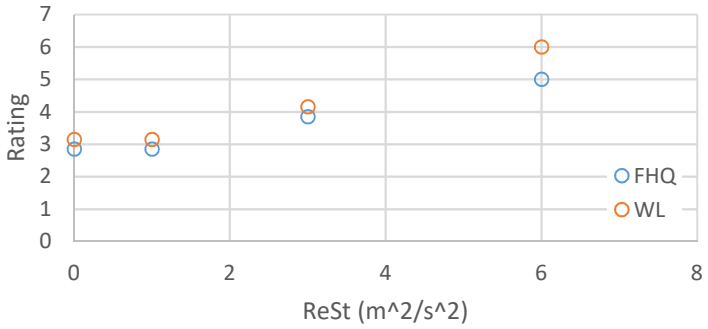

Figure 11: Pilot Flight handling qualities (FHQ) and workload (WL) ratings against magnitude of Reynolds stresses.

According to the pilot, when flying under turbulence, control in the vertical axis was the main driver for workload increases, followed by heading due to the resulting cross couplings. In the run under the highest turbulence intensity (Run 7, Reii = 6 (m^2/s^2)), the pilot indicated that lateral control required most of his effort, followed by heave and yaw. His comments suggest that vertical turbulence was probably too high for the low altitude setting of the precision hover MTE, although it might be more realistic in situations farther away from the ground like wind turbine servicing or hovering near cliffs. It also bears mention that the aircraft lacks any stability augmentation in heave, leaving the task of counteracting vertical disturbances entirely to the pilot. The impact of turbulence was more strongly felt during the hover phase, which on its own is more stabilization focused than the guidance focused translation phase.

Figure 12 a) shows aircraft ground track during approach to the hover point and Figure 12 b) shows approach rate to the hover point during the entire run (derivative of distance to the hover point with time) and c) shows altitude deviation from hover point during the entire run. As can be seen, the pilot was able to maintain course and approach rate with ease, with little deviations along the ground track and only slight oscillations in the approach rate for Run 7 with the highest turbulence intensity of Re_{ii} = 6 (m^2/s^2). The case is different when comparing altitude deviations. The pilot started the MTE slightly above the hover point and in all cases starts the approach with a slight climb which he corrects once near the hover point. This climb and the altitude oscillations during the approach become greater with increases in turbulence intensity, confirming pilot comments that put heave control as being the main driver of additional workload.

A smaller effect of the turbulence during the translation phase is consistent previous findings [26] and again might be a combination of the aircraft being less susceptible to disturbances during forward flight and that there are no requirements set for the translation phase of the hover MTE other than reaching the hover point in a single smooth maneuver.

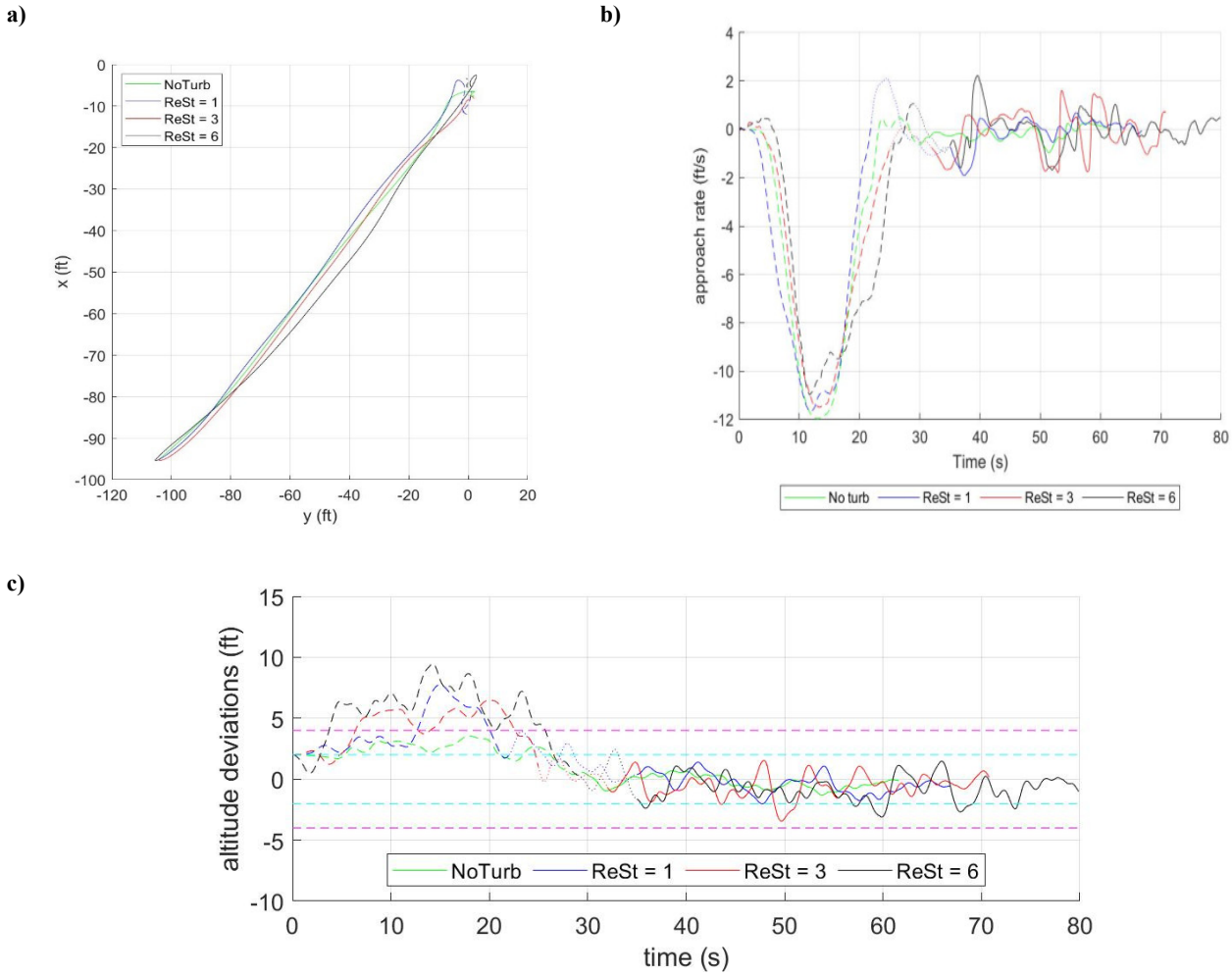

Figure 12: Approach to hover point: a) Groundtrack, b) approach rate to hoverpoint during the entire run, c) altitude deviations from hover altitude during the entire run. Approach, stabilization and hover phase are indicated in b) and c) by dashed, dotted and continuous lines respectively.

Figure 13 and Figure 14 show the performance achieved during the hover phase of the MTE and depict deviations in aircraft altitude, heading and ground position against ADS-33 defined adequate and desired performance boundaries. When flying without turbulence, the pilot shows no difficulty in keeping deviations within the desired boundaries. Under conditions of turbulence, amplitude of upsets increases and performance worsens, although deviations are kept within adequate limits most of the time. A rightward shift in heading (Figure 13 a) and b)) and larger oscillations in altitude (Figure 13 a) and c)) can be appreciated, although there seems to be a limited effect from increases in turbulence intensity. By contrast, deviations in longitudinal position (Figure 14 a) and b)) seem to be affected by the intensity of the turbulence, with adequate boundaries being exceeded in Run 7 under a turbulence of Re_{ii} = 6 (m^2/s^2) and deviations in lateral position increasing suddenly for this same run (Figure 14 a) and c)).

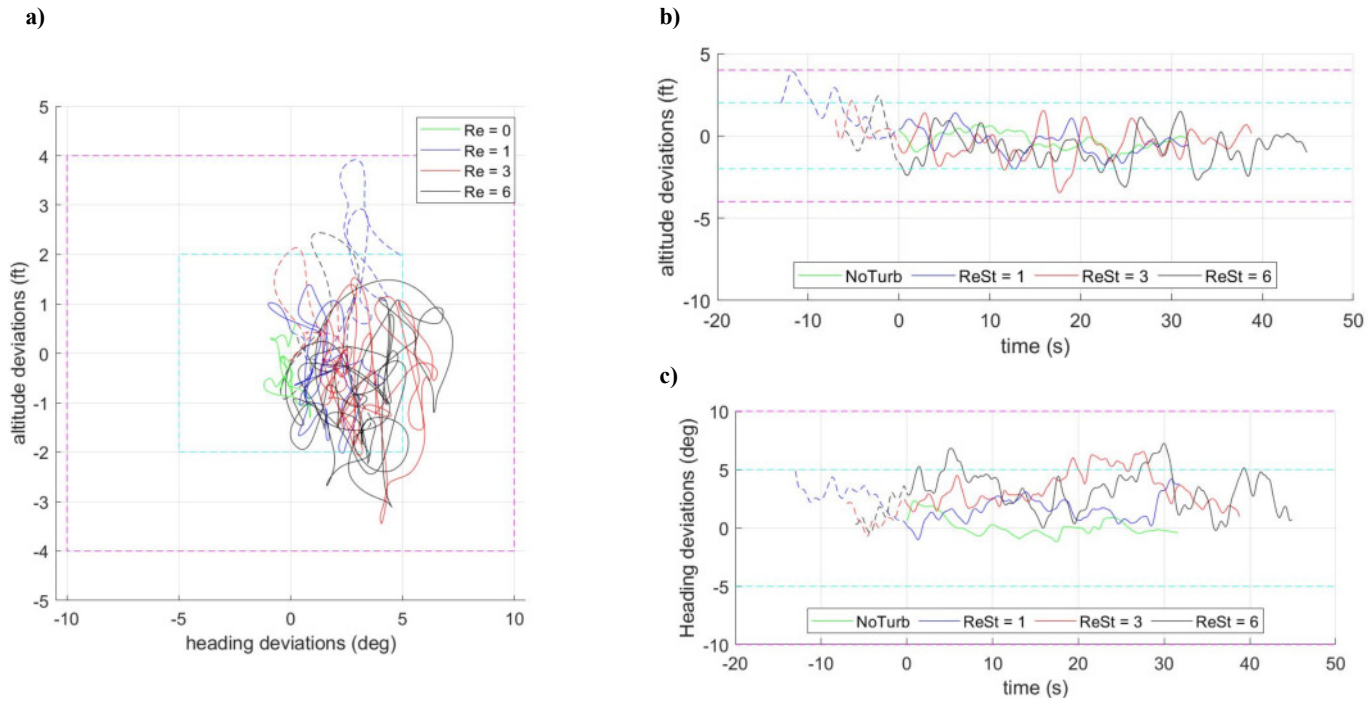

Figure 13: Altitude and heading deviations during the hover task for runs 2, 4, 6 and 7. Effect of eddy strength. Dashed lines indicate stabilization phase when applicable. Cyan and magenta dashed lines indicate desired and adequate boundaries. For time plots, 0 is moment when pilot declares aircraft to be stabilized.

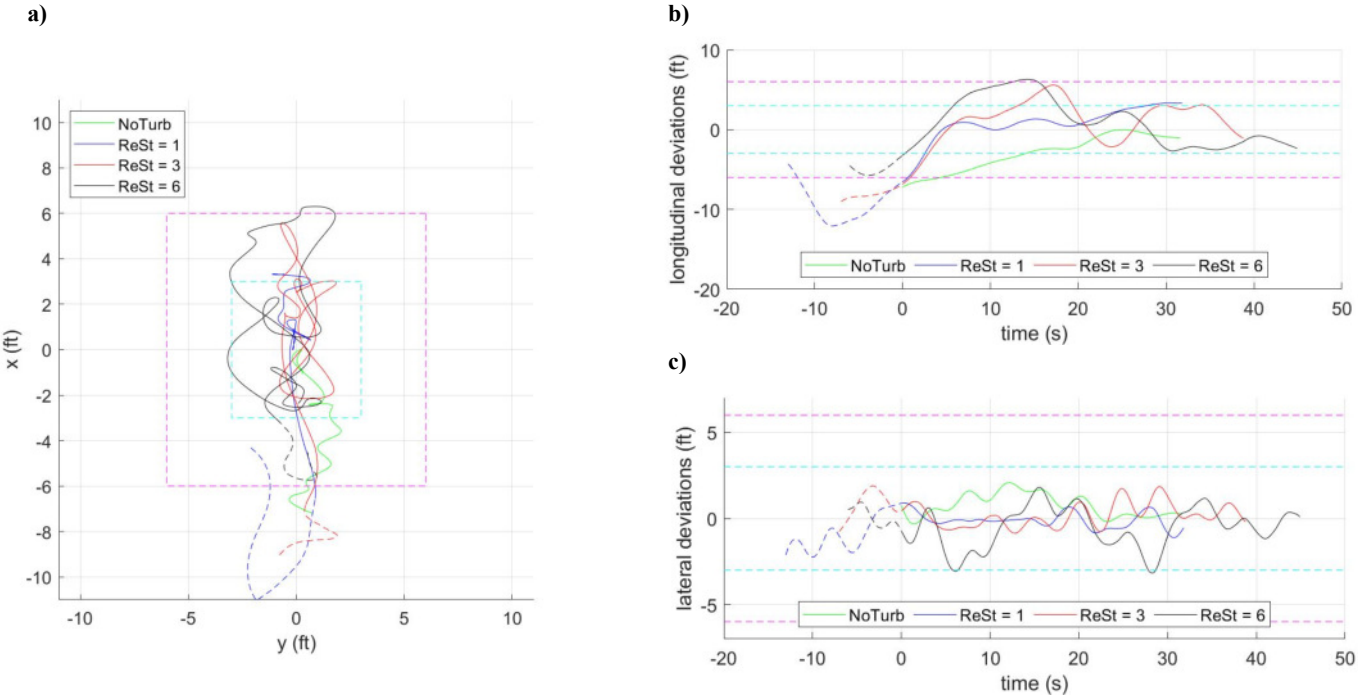

Figure 14: Longitudinal and lateral deviations during the hover task for runs 2, 4, 6 and 7. Effect of eddy strength. Dashed lines indicate stabilization phase when applicable. Cyan and magenta dashed lines indicate desired and adequate boundaries. For time plots, 0 is moment when pilot declares aircraft to be stabilized.

Power spectral density plots of pilot inputs during translation and hover are shown in Figure 15 and Figure 16 respectively. A clear increase in the amplitude of pilot inputs in all axis with increasing levels of turbulence intensity can be appreciated. A shift in control activity can also be appreciated between the two phases. During the run without any turbulence, translation to the hover point requires inputs in all axis (Figure 15), while hover seems to put demands mainly in lateral control (Figure 16 a) due to the lateral wind, with amplitude of inputs in all other axis decreasing. There is also a shift towards a higher input frequency, signaling a shift from guidance actions toward stabilization, the exception to this is the

lateral axis, probably due to the need to counteract the uniform lateral wind. The inclusion of turbulence seems to strongly change the nature of the task. The large amplitude increase in stick inputs during the translation phase for the lowest turbulence case (run 4, Re_{ii} = 1 m^2/s^2) stands out immediately, but this seems to be an outlier and might be because the pilot still needed to familiarize himself with the turbulence and resulting aircraft response and the effect seems to subside once the aircraft reaches the hover phase (Figure 16). Turbulence of intermediate intensity (run 6, Re_{ii} = 3 m^2/s^2) seems to have less effect during the translation phase, requiring some stabilization effort in heave (Figure 15 c) and larger pedal inputs (Figure 15 d) than the case without turbulence. However, there is a strong effect during the hover phase, with all axis requiring inputs of increasing amplitude. This increase in amplitude happens mainly in the 0Hz – 0.25Hz range for most axes. But collective inputs cover a wider frequency range between 0Hz to 0.6Hz already under conditions of no turbulence and the amplitude of pilot inputs grows across this entire range. When flying under the highest turbulence intensity (run 7, Re_{ii} = 6 m^2/s^2), the effect in hover is very similar to the previous case, however longitudinal and collective inputs during the translation phase cover a wider range of frequencies, again pointing towards a larger stabilization effort from the pilot.

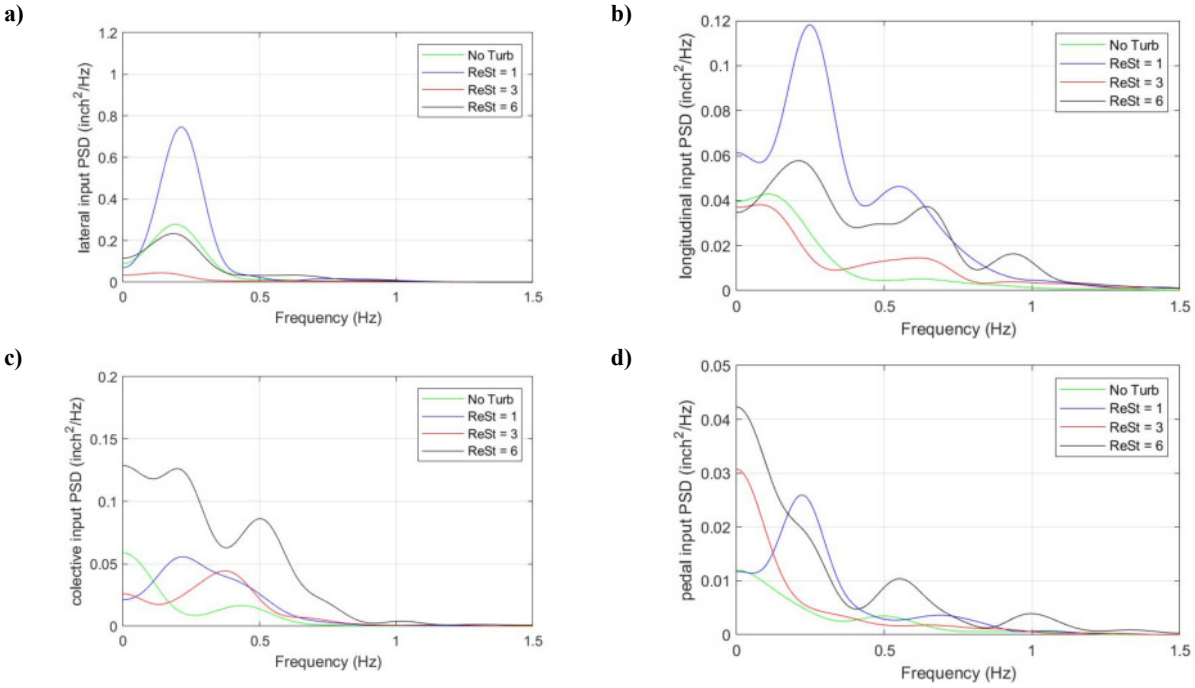

Figure 15: Power spectral density of pilot inputs during translation to hover point: in a) lateral, b) longitudinal, c) collective, d) pedal.

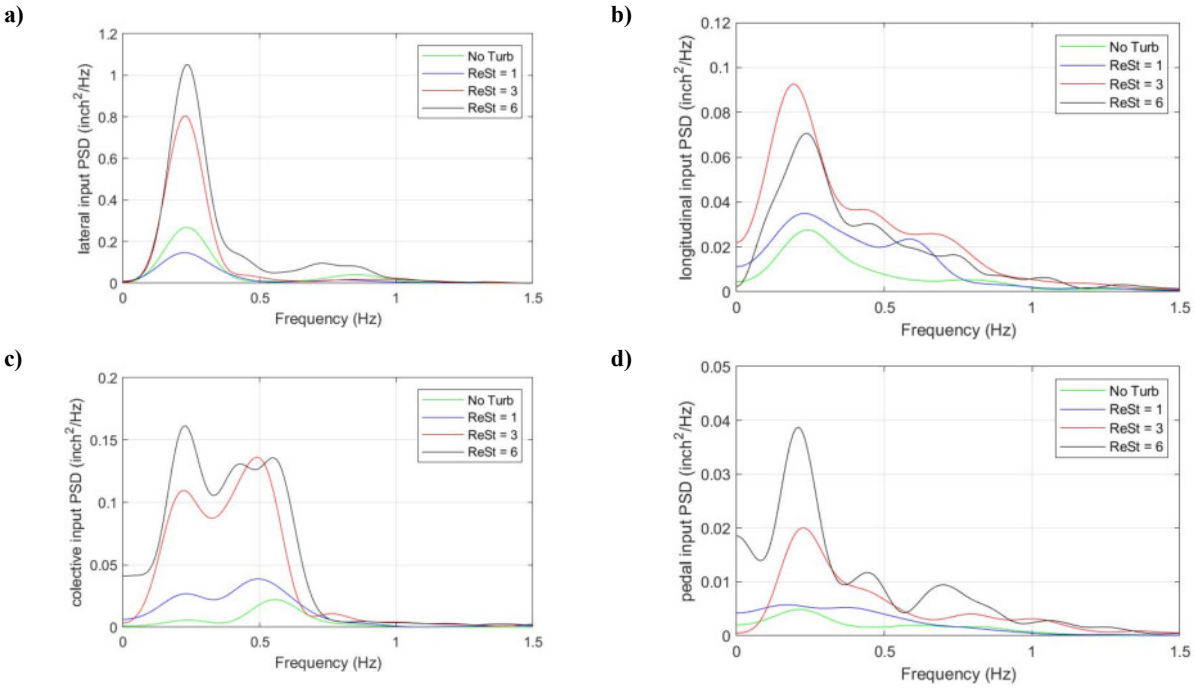

Figure 16: Power spectral density of pilot inputs during station keeping over hover point: in a) lateral, b) longitudinal, c) collective, d) pedal.

The stabilization phase of the task was identified during the tests by the pilot announcing when the aircraft had reached the hover point and when stabilized hover had been achieved. The time required to stabilize the aircraft over the hover point was measured from the voice recordings taken during the test and varies wildly by case. With the exception of a 13s long stabilization period for run 4 (Re_{ii} = 1 m^2/s^2) which again seems to be an outlier, stabilization was usually achieved within the adequate time limits and was reached immediately upon reaching the hover point for the case without turbulence (run 2, Re_{ii} = 0 m^2/s^2).

There seems to be no strong correlation between time required for stabilization and pilot ratings or turbulence parameters nor clear cues of stabilization maneuvers that can be inferred from recorded pilot inputs and aircraft behavior and used to separate this phase from translation and hover. Figure 17 shows pilot inputs for the entirety of runs 4, 5 and 7 (Re_{ii} = 1 m^2/s^2, Re_{ii} = 3 m^2/s^2 and Re_{ii} = 6 m^2/s^2), with discontinuous, dotted and continuous lines indicating the translation, stabilization and hover respectively. Some of the patterns in pilot inputs distinguishing the translation and hover phases identified in the PSD plots of Figure 15 an Figure 16 can be identified here too, including a trend of larger inputs under turbulence, larger higher frequency inputs during the hover phase and the increased demands for collective and lateral control under turbulence and there seem to be some large single pilot inputs during the transition period or just entering it (lateral inputs for runs 4 and 7, longitudinal inputs for run 4 and collective inputs for run 7).

However, these are of similar size than later inputs during the hover phase. This seems to suggest that the presence of turbulence requires a constant stabilization effort on the part of the pilot to compensate from turbulence induced disturbances and that it might not make sense to separate the stabilization phase from hover. If this is the case, the stabilization time requirement will be dropped for future testing.

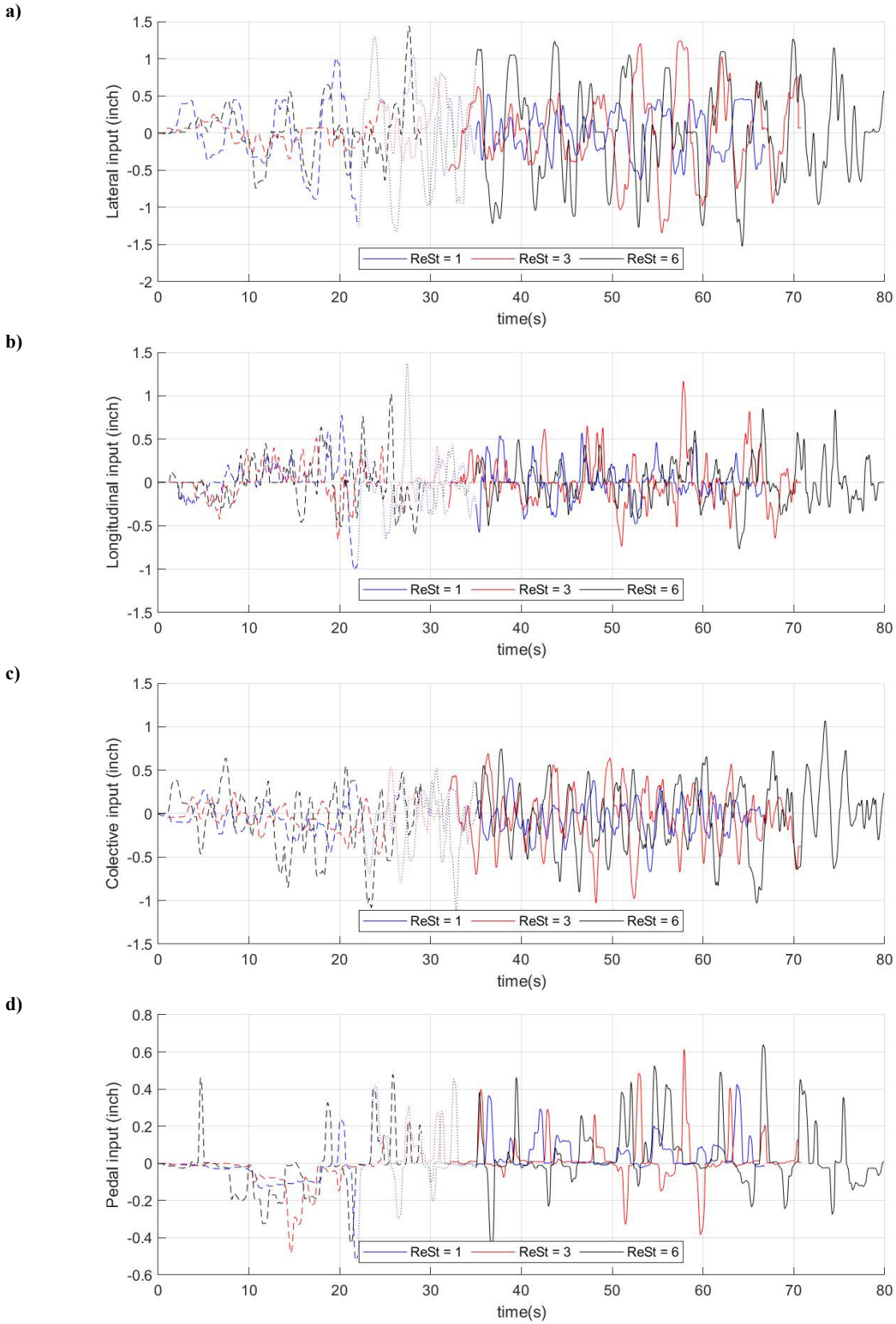

Figure 17: Pilot inputs during runs 4 (Re_{ii} = 1), 6 (Re_{ii} = 3) and 7 (Re_{ii} = 6) in a) lateral, b) longitudinal, c) collective and d) pedal. Approach, stabilization and hover phases are given by dashed, dotted and continuous lines respectively.

Previous work [39], [40], [26] has shown a correlation between pilot workload ratings and root mean square (RMS) values of oscillations in aircraft forces and moments. This value is defined as the root

square of power spectral density between the frequencies of 0.1Hz and 2Hz. Figure 18 shows RMS values of oscillations in aircraft moments and forces against values of Re_{ii} for the translation and hover phases of the MTE. An increase in RMS values with turbulence intensity can be appreciated, especially for vertical and lateral forces. There is little difference in RMS values between the translation and hover phases except for vertical and lateral forces which seem to be less affected during run 5 of intermediate turbulence intensity, Re_{ii} = 3 m^2/s^2.

RMS of pilot inputs are shown in Figure 19 a) for stick inputs and Figure 19 b) for collective and pedal inputs. Predictably pilot inputs follow the same trend of increasing RMS values with turbulence intensity as moments and forces, with the already mentioned exception of the translation phase of run 4 (Re_{ii} = 1 m^2/s^2).

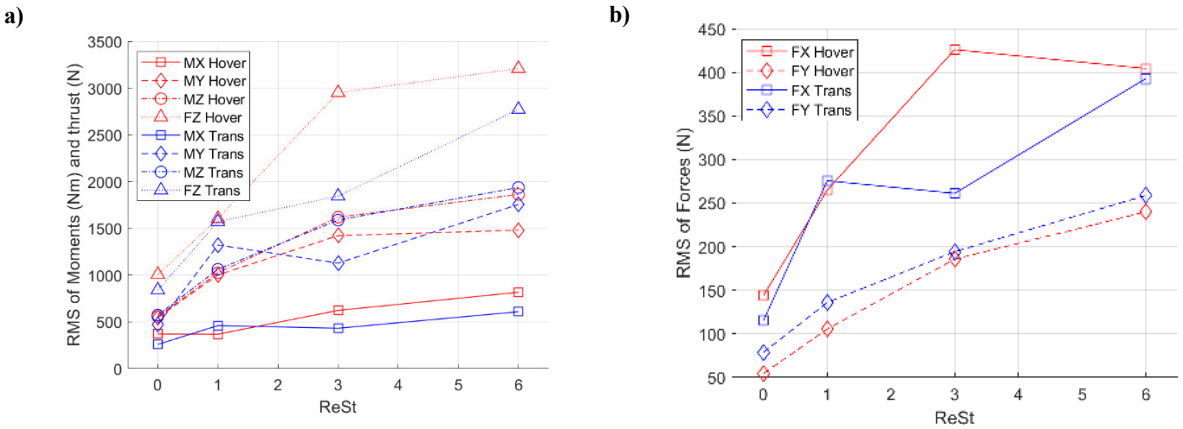

Figure 18: Root mean square of oscillations in aircraft a) moments and vertical force, b) longitudinal and lateral forces

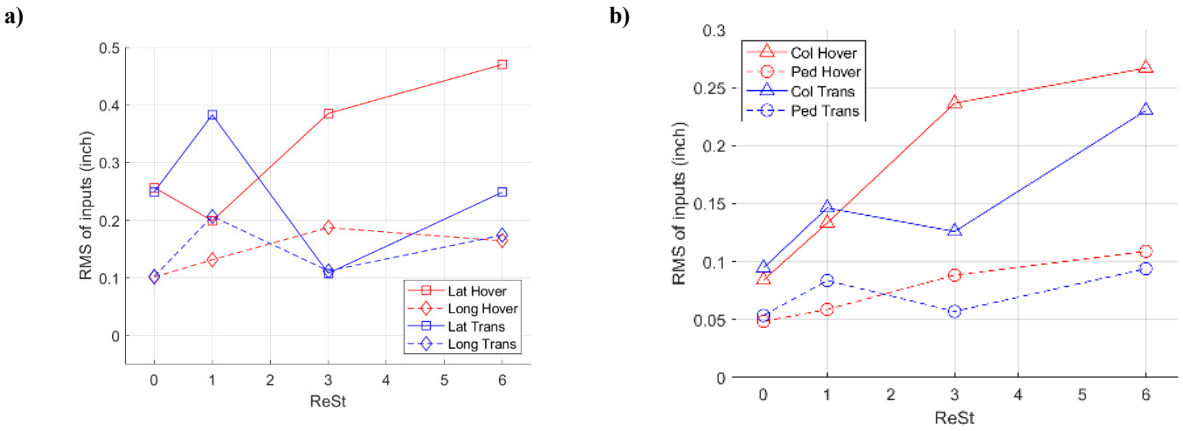

Figure 19: Root mean square of pilot inputs: a) in lateral and longitudinal, b) in collective and pedal.

Effect of eddy size

In order to test the impact on aircraft response and pilot workload of increasing the size of turbulent eddies, runs 6 and 8 were performed with eddy sizes of σ_i = 6m and σ_i = 9m, resulting in turbulence of lower average frequency. All tests were performed under Reynolds stress values of Re_{ii} = 3 m^2/s^2. The pilot awarded higher FHQ and WL ratings when flying within turbulence of increasing eddy sizes, as can be seen in Figure 20. For run 8 with eddy size of σ_i = 9m, the pilot awarded a level 2 FHQ rating of 6 and a level 3 WL rating of 7 implying extensive pilot effort required for the main task and very little spare capacity available, although the primary task of flying the MTE was not in question.

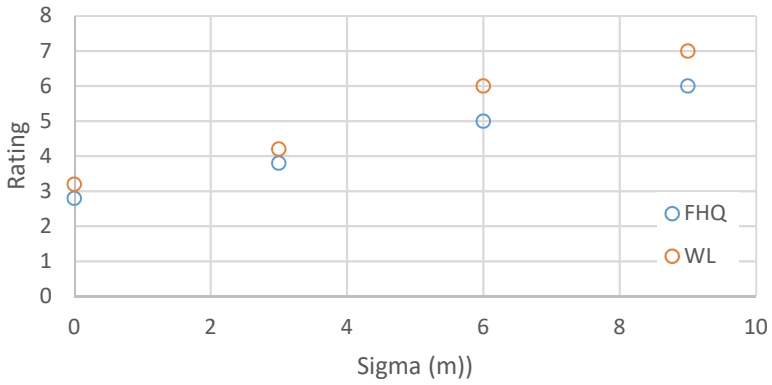

Figure 20: Pilot Flight handling qualities (FHQ) and workload (WL) ratings against eddy size.

Heave control was again cited by the pilot as the main driver of workload increases in all flights, with compensation of cross couplings in yaw being the secondary cause. The exact character of resulting aircraft disturbance however seems to change under different eddy sizes. During run 6, with σ_i = 6m, the pilot reported difficulty in maintaining a constant approach rate during the translation to hover phase and a reduced predictability of aircraft responses to collective inputs. Suggesting a certain delay in aircraft response, leading to excessive inputs. In the case of run 8 with σ_i = 9m the pilot declared that the high FHQ and WL ratings were driven by possible pilot induced oscillations (PIO) in the collective axis that occurred during the last 10 seconds. For the entirety of the run before the possible PIO, the pilot considered the most important upsets during the run to be in the heave axis and easily controllable despite a slow aircraft response to collective input.

Ground track during approach to hover, as well as approach rate and altitude over the hover point during the entire run are shown in Figure 21 a), b) and c) respectively. The most interesting case is run 6 (σ_i = 6m). Not only did the translation phase for this run take significantly more time than for other cases, it also shows important oscillations in approach rate and a significant climb during the translation to the hover point of around 5ft in above what is seen for other cases. Run 8 with σ_i = 9m shows again a profile similar to the other runs regarding approach rate and altitude oscillations.

a)

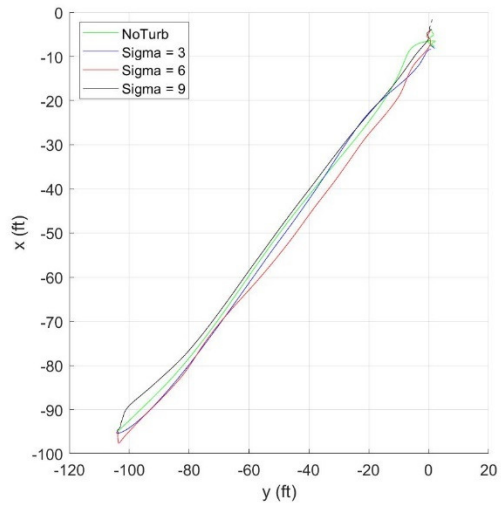

b)

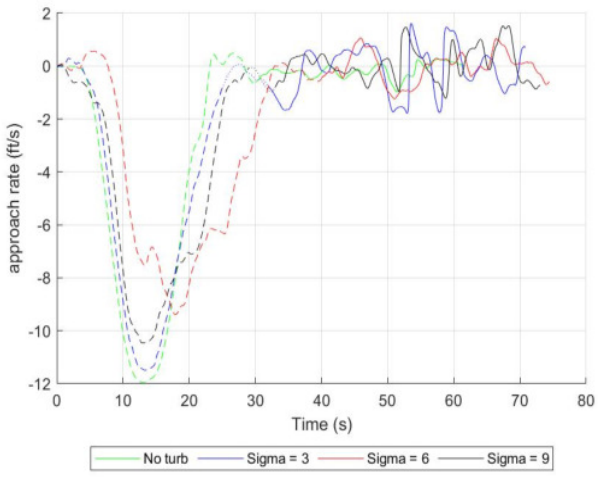

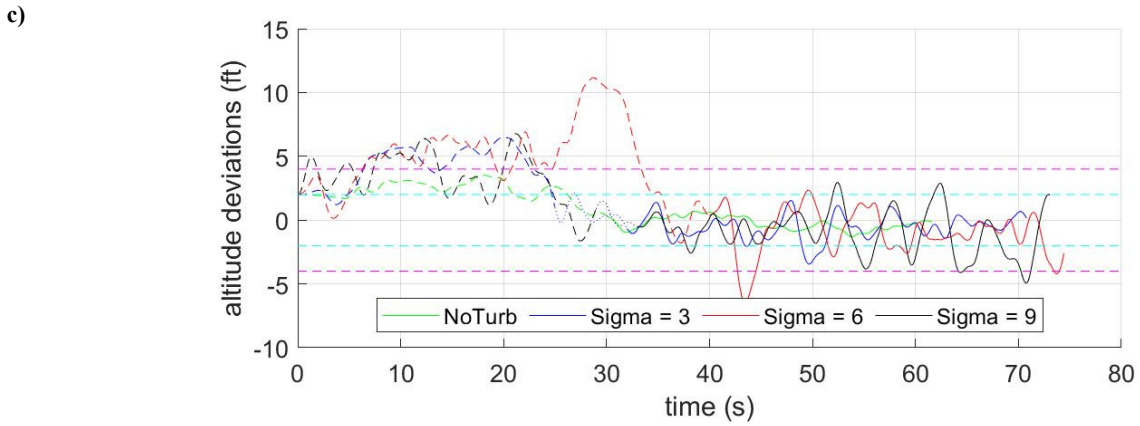

Figure 21: Approach to hover point: a) Groundtrack, b) approach rate to hoverpoint during the entire run, c) altitude deviations from hover altitude during the entire run. Approach, stabilization and hover phase are indicated in b) and c) by dashed, dotted and continuous lines respectively.

Task performance during the hover phase is shown in Figure 22 and Figure 23. Figure 22 depicts altitude and heading deviations during runs 4 (no turbulence), 5 (σ_i = 3m), 6 (σ_i = 6m) and 8 (σ_i = 9m). As can be seen, adequate performance was achieved for most of the time in all runs, with heading deviations being kept mostly within the desired range. Oscillations in heave (Figure 22 b) present the most interesting trend with one very large descend outside the adequate range evident for run 6 (σ_i = 6m) and a series of large oscillations between seconds 20 and 30 of run 8 (σ_i = 9m), which occur in the time period for which the pilot might have encountered a possible PIO. Deviations in longitudinal and lateral position are shown in Figure 23. Deviations in longitudinal position (Figure 23 b) are kept mainly within adequate boundaries, although all runs present a soft, oscillating forward shift. The pilot manages to keep lateral deviations (Figure 23 c) within desired boundaries in all cases, except during the last 10 seconds of run 8 (σ_i = 9m), when the aircraft drifts slightly to the left.

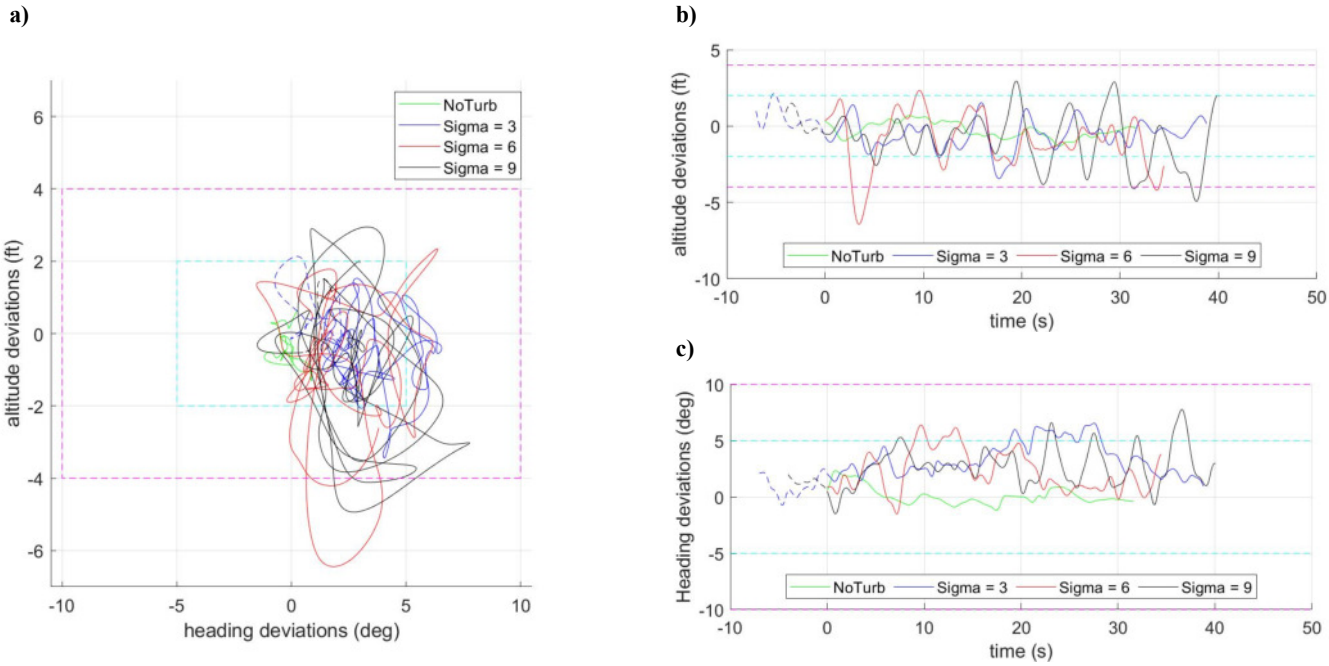

Figure 22: Altitude and heading deviations during the hover task for runs 2, 5, 6 and 8. Effect of eddy strength. Dashed lines indicate stabilization phase when applicable. Cyan and magenta dashed lines indicate desired and adequate boundaries. For time plots, 0 is moment when pilot declares aircraft to be stabilized.

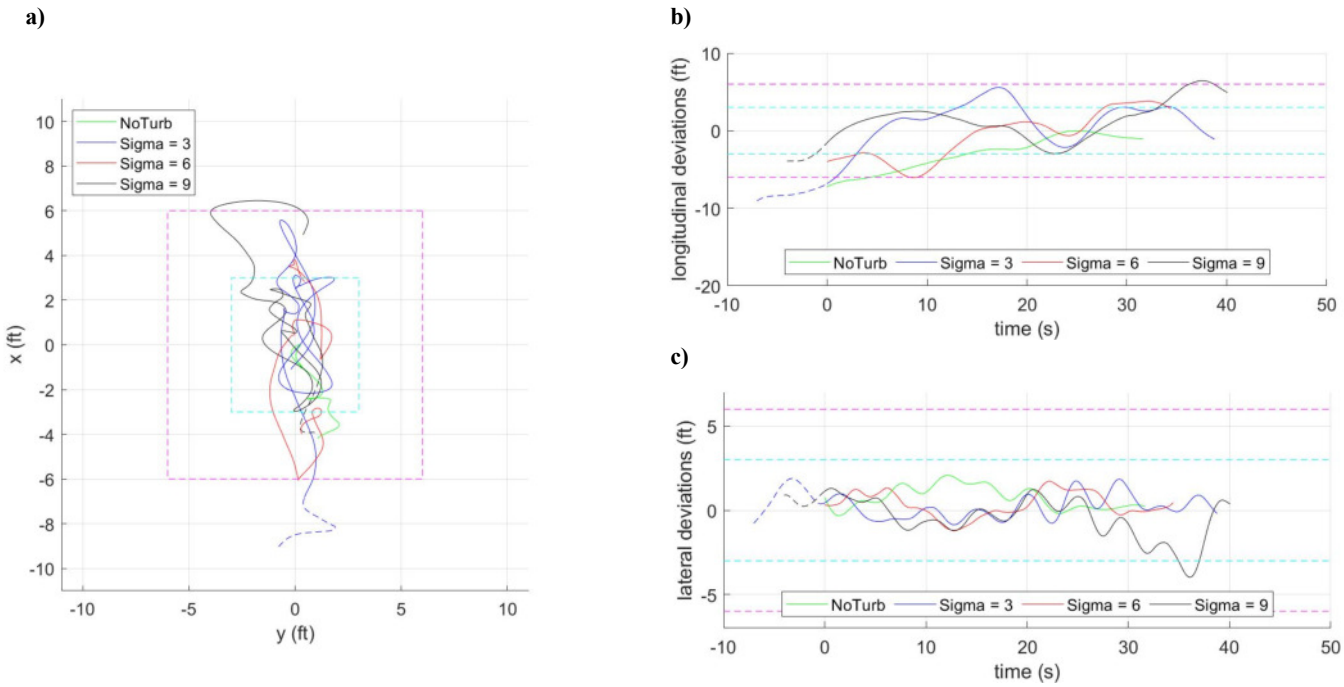

Figure 23: Longitudinal and lateral deviations during the hover task for runs 2, 4, 6 and 7. Effect of eddy strength. Dashed lines indicate stabilization phase when applicable. Cyan and magenta dashed lines indicate desired and adequate boundaries. For time plots, 0 is moment when pilot declares aircraft to be stabilized.

PSD plots of pilot inputs during the translation and hover phases are shown in Figure 24 and Figure 25 respectively. During run 6, when flying under turbulence of eddy size σ_i = 6m, the pilot needed to produce inputs of very large amplitude during the translation phase, mainly in the lateral (Figure 24 a) and longitudinal (Figure 24 b) axis. Inputs on the longitudinal axis also cover a broad frequency spectrum of 0 to 0.75Hz with peaks at around 0.25 Hz and 0.6 Hz, suggesting a mixture of guidance and stabilization pilot activity, something often associated with large workload increases [43]. Pilot inputs in collective and pedal also show a small increase in amplitude and cover a wider frequency range of between 0Hz and 0.5Hz than under smaller eddy sizes. By contrast, during run 8, flown under turbulence of eddy size of σ_i = 9m, pilot stick inputs do not present such large amplitudes and collective and pedal inputs show a very similar behavior as in the case of σ_i = 6m.

During the hover phase pilot inputs present a pattern similar to the one observed previously with increases in turbulence intensity. Lateral and longitudinal inputs (Figure 25 a) and b) show an increase in amplitude with smaller eddy sizes, while the opposite is true for inputs in collective and pedal (Figure 25 a) and b).

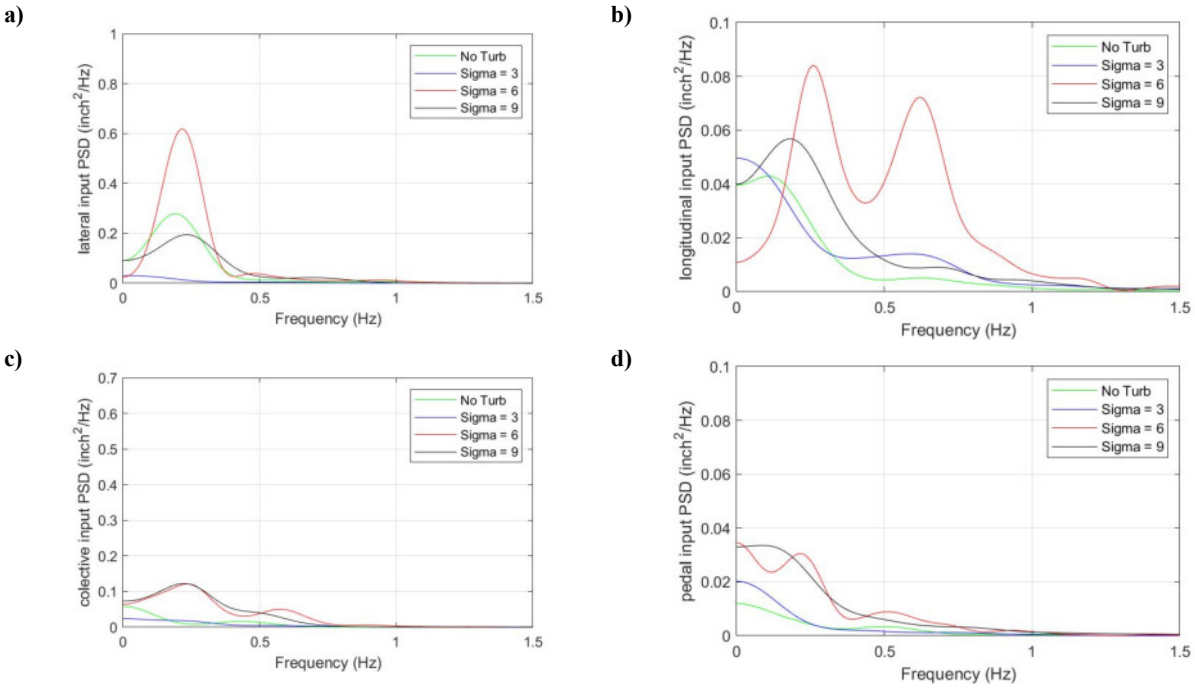

Figure 24: Power spectral density of pilot inputs during translation to hover point: in a) lateral, b) longitudinal, c) collective, d) pedal.

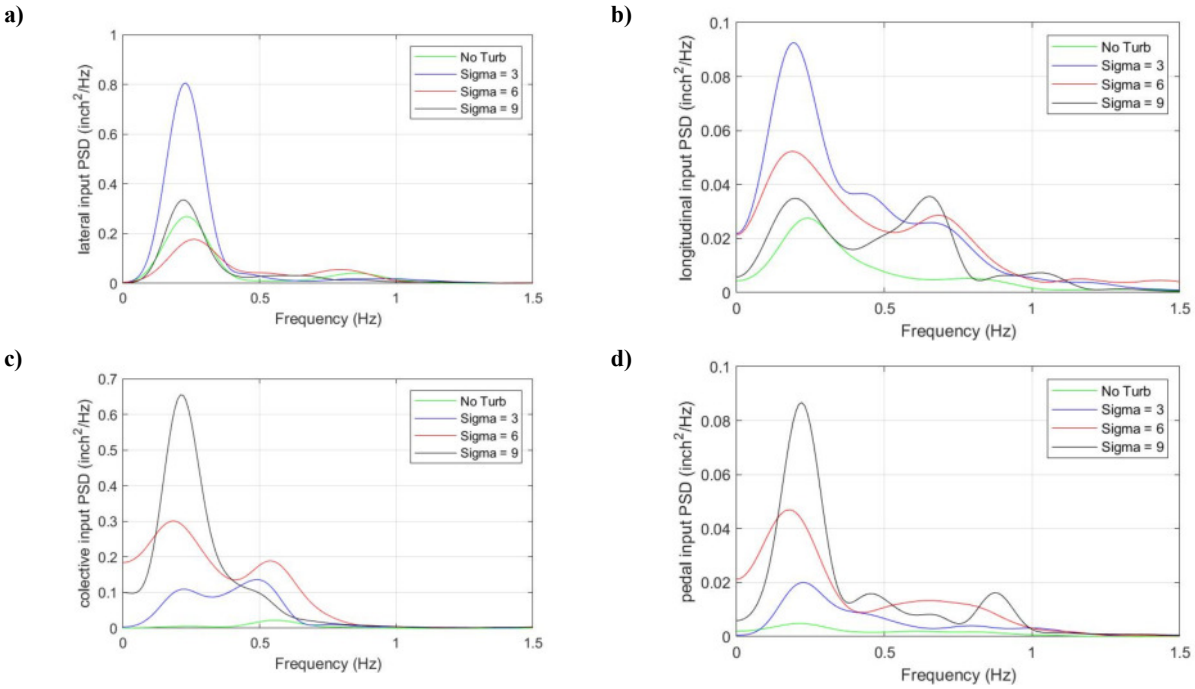

Figure 25: Power spectral density of pilot inputs during station keeping over hover point: in a) lateral, b) longitudinal, c) collective, d) pedal.

The pilot commented that he encountered a possible PIO in the heave axis at the end of the station keeping phase of run 8 (eddy size σ_i = 9m). Figure 26 depicts pilot inputs in the collective together with altitude deviations over the hover point and seems to confirm this. Some 17 seconds after the start of the hover, the pilot started introducing large inputs into the collective which follow a 180 deg phase delay with large oscillations in altitude occurring during the same time period. This situation lasts until almost 35 seconds into the hover phase. Interestingly, this phase delay seems to be present already from the start of the hover phase, although oscillations are of much smaller amplitude.

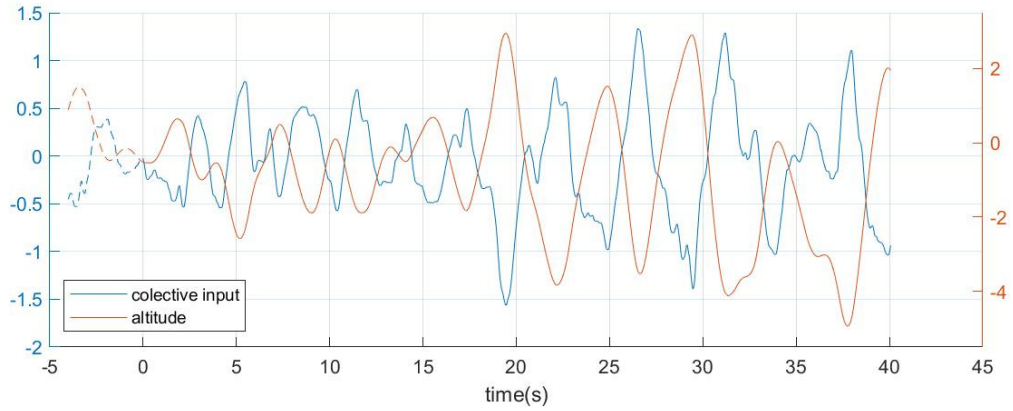

Figure 26: Left axis: pilot inputs in collective during the hover phase. Right axis: altitude deviations from hover point during hover phase. Discontinuous lines mark the stabilization phase.

The duration of the stabilization phase during runs 6 and 8 also seems to present very little correlation with eddy size or awarded pilot rating and will not be discussed in this section.

RMS of oscillations in moments and forces acting on the aircraft against values of eddy size are shown in Figure 27 a) and b) respectively. During translation, RMS values of pitch moment as well as vertical and longitudinal forces show a peak at eddy sizes of σ_i = 6m, while roll and yaw moments show little effect from the changes in eddy size. For the hover phase, RMS values for vertical and longitudinal forces show important increases with eddy size a slight decrease in roll moments and slight increases for all other forces and moments. Changes in RMS values when switching from translation to hover can also be seen, usually as increases in RMS values, with the most notable being large increases for vertical and longitudinal forces. An decrease in RMS values for for pitch moments and longitudinal forces for eddy sizes σ_i = 6m can also be appreciated after transitioning into the hover phase.

a) **b)**

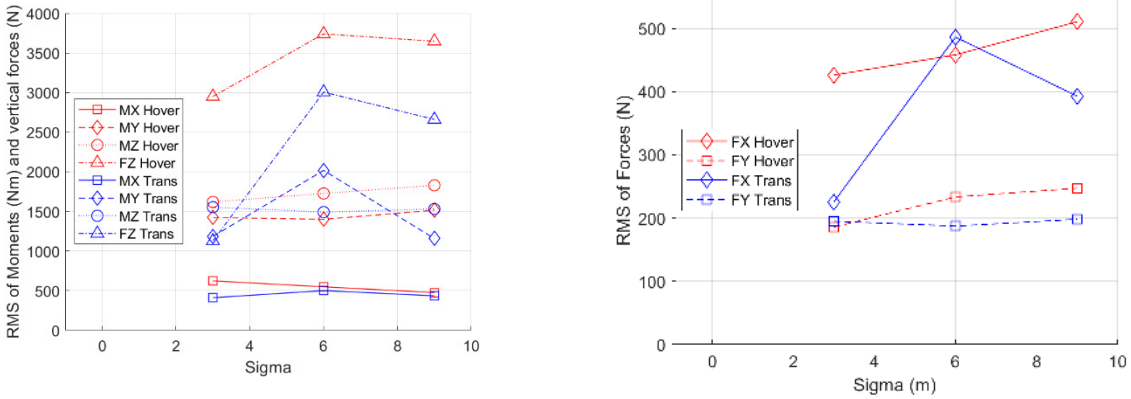

Figure 27: Root mean square of oscillations in aircraft a) moments and vertical force, b) longitudinal and lateral

RMS values of pilot inputs are shown Figure 28 and do not follow RMS of forces and moments as closely as observed when changing the values of Reynolds stresses (which were shown in Figure 19). Stick inputs (Figure 28 a) during translation present a peak in RMS value for run 6 at eddy size of σ_i = 6m, especially in the lateral axis despite there being no such large increases in RMS values of roll moments and lateral forces. During the hover phase, the trend for lateral and longitudinal inputs becomes the inverse with highest RMS values appearing at σ_i = 3m. Pilot inputs in collective (Figure 28 b) seem to follow the same behavior as oscillations in vertical forces, presenting a large increase when shifting from translation to hover phase. Pedal inputs also show an increase with eddy size despite there being little change in RMS values of yaw moment, which might be a consequence of cross couplings with the collective.

a)

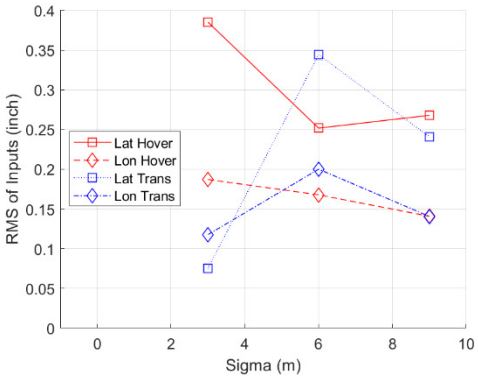

b)

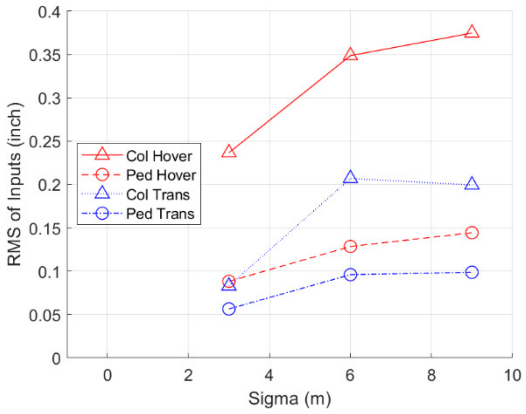

Figure 28: Root mean square of pilot inputs: a) in lateral and longitudinal, b) in collective and pedal.

Discussion and future work

The previous paper presents some initial results from the analysis of an ongoing simulation test campaign of a new turbulence model based on a synthetic eddy method. The main aim is to better understand turbulence induced disturbances of the model in order to improve calibration of the model and achieve a better representation of real-world conditions.

Two main turbulence parameters have been the focus of this analysis, Reynolds stress, which regulate turbulence intensity and eddy size which affects the frequency of the resulting turbulence and their impact on handling during an ADS - 33 precision hover MTE has been assessed. As a general trend, the presence of turbulence results in a worsening of aircraft handling, an increase in pilot workload and a reduction in task performance. With the effects becoming more severe as the values of Reynolds stresses and eddy size increase.

Without turbulence the pilot considered control in the lateral and longitudinal axis to be the main drivers for workload during the task. When flying under SEM induced turbulence, control in heave became the main workload driver in most cases. Possible causes for this might be the lack of any stability augmentation in the heave axis for the Bell412 as well as the close proximity to the ground. Pilot comments suggest that the vertical turbulence might have been too high when compared with lateral gust for what would be expected at such close proximity to the ground.

Assessing transition from translation to hover according to the stabilization time criteria defined in ADS – 33 proved difficult. It is hard to clearly determine where the stabilization phase ends and station keeping starts. The presence of turbulence requires constant stabilization effort on the part of the pilot and separating the two phases might not make sense when assessing task performance.

Flying under increasing values of Reynolds stress tensor while maintaining a small eddy size (σ_i = 3m), leads to increases in workload requirements and decreasing task performance. The effect seems to be greater during the hover phase than for the translation phase due to a combination of stricter task requirements and greater aircraft susceptibility to disturbances. The greater workload seems to be due to need for the pilot to generate stabilization inputs of larger amplitude in the heave axis. Under the highest value of Reynolds stress tested (Re_{ii} = 6 m^2/s^2), the large amplitude of required lateral inputs took over as the main driver of pilot workload increases. The trend found during the feasibility test of increasing RMS values for moments, forces and pilot inputs when increasing turbulence intensity is also confirmed here for the larger Reynolds stress values tested.

Keeping the value of Reynolds stresses constant while increasing the eddy size also leads to an increase in workload requirements and worse task performance, although of a different nature. When flying under an eddy size of σ_i = 6m, pilot workload increases seemed to occur mainly during the translation to the hover point. He encountered difficulties in attempting to maintain a constant approach rate and altitude to the hover point. Analysis of pilot inputs suggest an increased need of guidance inputs during the translation phase, while pilot comments suggest that response to collective inputs becomes less predictable. Increasing eddy size further to σ_i = 9m seems to reduce the effect of

turbulence during the translation phase, however induced disturbances during the hover phase seem to put the aircraft and pilot into PIO prone situations. The trend that might relate workload with RMS values of moments and forces for increasing levels of turbulence intensity does not seem to be valid when dealing with turbulence eddy size, RMS for vertical and longitudinal forces as well as pitch moments during translation still show a peak for σ_i = 6m.

Future work should focus on continuing simulation testing of the model in order to better understand its effects on pilot workload and improving its calibration. An adequate relationship between the different velocity components in all three axis shall be found that better corresponds to turbulence conditions at the simulated altitude. Also, the relationship between the frequency of disturbances, flight conditions and effect on workload shall be further explored. This will be the aim of future testing currently being planned.

References

[1] G. Quaranta, M. Pavel, G. Barakos, M. White, and M. Mulder, "NITROS : An Innovative Training Program to Enhance Rotorcraft Safety," *AHS Int. 74th Annu. Forum Technol. Disp.*, 2018.

[2] I. Owen, M. D. White, G. D. Padfield, and S. J. Hodge, "A virtual engineering approach to the ship-helicopter dynamic interface – a decade of modelling and simulation research at the University of Liverpool," *Aeronaut. J.*, vol. 121, no. 1246, pp. 1833–1857, Dec. 2017, doi: 10.1017/aer.2017.102.

[3] UK Civil Aviation Authority, "CAA PAPER 2004/03 Helicopter Turbulence Criteria for Operations to Offshore Platforms," 2004.

[4] Y. Wang, M. White, and G. N. Barakos, "Wind Turbine Wake Encounter Study; University of Liverpool Report for CAA," 2015. doi: 10.1016/j.aqpro.2013.07.003.

[5] R. Bakker *et al.*, "Wind turbine wakes and helicopter operations, an overview of the GARTEUR HC-AG23 activities," *44th Eur. Rotorcr. Forum*, 2018.

[6] *CS - 27 Certification Specifications and Acceptable Means of Compliance for Small Rotorcraft*. European Aviation Safety Agency, 2016.

[7] *CS - 29 Certification Specifications and Acceptable Means of Compliance for Large Rotorcraft*. European Aviation Safety Agency, 2016.

[8] "Aeronautical Design Standards - Performance Specification Handling Qualities Requirements for Military Rotorcraft," *United States Army Aviat. Missile Command*, vol. E-PRF, 2000.

[9] R. H. Hoh, D. G. Mitchell, B. L. Aponso, D. L. Key, and C. Blanken L., "Special Report RDMR-AD-16-01: Background Information and User's Guide for Handling Qualities Requirements for Military Rotorcraft," *Aviat. Dev. Dir. Ames Res. Cent.*, 1989, [Online]. Available: https://apps.dtic.mil/dtic/tr/fulltext/u2/1000418.pdf.

[10] T. Berger, C. M. Ivler, M. G. Berrios, M. B. Tischler, and D. G. Miller, "Disturbance Rejection Handling Qualities Criteria for Rotorcraft," *Am. Helicopter Soc. 72nd Annu. Forum, West Palm Beach, FL*, 2016.

[11] UK Civil Aviation Authority, "CAP 437 Standards for Offshore Helicopter Landing Areas," 2013.

[12] U. C. A. Authority, "CAA Paper 2009 / 03: Offshore Helideck Environmental Research Part," 2009.

[13] G. H. Gaonkar, "Review of Turbulence Modeling and Related Applications to Some Problems of Helicopter Flight Dynamics," *J. Am. Helicopter Soc.*, vol. 53, no. 1, p. 87, 2008, doi: 10.4050/JAHS.53.87.

[14] T. von Karman, "Progress in the Statistical Theory of Turbulence," *Proc. Natl. Acad. Sci.*, vol. 34, no. 11, pp. 530–539, Nov. 1948, doi: 10.1073/pnas.34.11.530.

[15] H. L. Dryden, "A review of the statistical theory of turbulence," *Q. Appl. Math.*, vol. 1, no. 1, pp. 7–42, Apr. 1943, doi: 10.1090/qam/8209.

[16] B. Etkin, “Turbulent Wind and Its Effect on Flight,” *J. Aircr.*, vol. 18, no. 5, pp. 327–345, May 1981, doi: 10.2514/3.57498.

[17] Mark F. Costello, “A Theory for the Analysis of Rotorcraft Operating In Atmospheric Turbulence,” *Am. Helicopter Soc. 46th Annu. Forum, Wahsingt. DC*, pp. 1689-, 1990.

[18] Y. Y. Dang, S. Subramanian, and G. H. Gaonkar, “Modeling Turbulence Seen by Multibladed Rotors for Predicting Rotorcraft Response with Three-Dimensional Wake,” *J. Am. Helicopter Soc.*, vol. 42, no. 4, pp. 337–349, 2009, doi: 10.4050/jahs.42.337.

[19] R. E. Mcfarland and K. Duisenberg, “NASA Technical Memorandum 108862: Simulation of rotor blade element turbulence,” Moffett Field, CA, 1995.

[20] H. Ji, R. Chen, and P. Li, “Distributed atmospheric turbulence model for helicopter flight simulation and handling-quality analysis,” *J. Aircr.*, vol. 54, no. 1, pp. 190–198, 2017, doi: 10.2514/1.C033667.

[21] J. A. Lusardi, M. B. Tischler, C. L. Blanken, and S. J. Labows, “Empirically Derived Helicopter Response Model and Control System Requirements for Flight in Turbulence,” *J. Am. Helicopter Soc.*, vol. 49, no. 3, pp. 340–349, 2009, doi: 10.4050/jahs.49.340.

[22] S. Seher-Weiss and W. Von Gruenhagen, “Development of EC 135 turbulence models via system identification,” *Aerosp. Sci. Technol.*, vol. 23, no. 1, pp. 43–52, 2012, doi: 10.1016/j.ast.2011.09.008.

[23] R. A. Hess, “Technical Note: A Simplified and Approximate Technique for Scaling Rotorcraft Control Inputs for Turbulence Modeling,” *J. Am. Helicopter Soc.*, vol. 49, no. 3, pp. 361–366, Jul. 2004, doi: 10.4050/JAHS.49.361.

[24] W. A. Memon, I. Owen, and M. D. White, “SIMSHOL: A Predictive Simulation Approach to Inform Helicopter–Ship Clearance Trials,” *J. Aircr.*, pp. 1–22, May 2020, doi: 10.2514/1.C035677.

[25] N. Jarrin, S. Benhamadouche, D. Laurence, and R. Prosser, “A synthetic-eddy-method for generating inflow conditions for large-eddy simulations,” *Int. J. Heat Fluid Flow*, vol. 27, no. 4, pp. 585–593, 2006, doi: 10.1016/j.ijheatfluidflow.2006.02.006.

[26] S. Henriquez Huecas, M. White, and G. Barakos, “A turbulence model for flight simulation and handling qualities analysis based on a synthetic eddy method,” *To be Present. 76th Vert. Flight Soc. Forum, Virginia Beach, VA*, 2020.

[27] N. Jarrin, R. Prosser, J. C. Uribe, S. Benhamadouche, and D. Laurence, “Reconstruction of turbulent fluctuations for hybrid RANS/LES simulations using a Synthetic-Eddy Method,” *Int. J. Heat Fluid Flow*, vol. 30, no. 3, pp. 435–442, 2009, doi: 10.1016/j.ijheatfluidflow.2009.02.016.

[28] Y. Luo, H. Liu, Q. Huang, H. Xue, and K. Lin, “A multi-scale synthetic eddy method for generating inflow data for LES,” *Comput. Fluids*, vol. 156, pp. 103–112, 2017, doi: 10.1016/j.compfluid.2017.06.017.

[29] Y. Luo, H. Liu, Q. Huang, H. Xue, and K. Lin, “A multi-scale synthetic eddy method for generating inflow data for LES,” *Comput. Fluids*, vol. 156, no. March 2019, pp. 103–112, 2017, doi: 10.1016/j.compfluid.2017.06.017.

[30] S. Henriquez Huecas, “Flight simulation testing of a turbulence model based on a Synthetic Eddy Method,” *46th Eur. Rotorcr. Forum, Sept. 2020, Moscow, Russ.*

[31] R. W. Du Val and C. He, “Validation of the FLIGHTLAB virtual engineering toolset,” *Aeronaut. J.*, vol. 122, no. 1250, pp. 519–555, Apr. 2018, doi: 10.1017/aer.2018.12.

[32] M. D. Pavel, M. White, G. D. Padfield, G. Roth, M. Hamers, and A. Taghizad, “Validation of mathematical models for helicopter flight simulators past, present and future challenges,” *Aeronaut. J.*, vol. 117, no. 1190, pp. 343–388, Apr. 2013, doi: 10.1017/S0001924000008058.

[33] G. Padfield and M. White, “Measuring simulation fidelity through an adaptive pilot model,” *Aerosp. Sci. Technol.*, vol. 9, no. 5, pp. 400–408, Jul. 2005, doi: 10.1016/j.ast.2005.03.004.

[34] P. Perfect, M. D. White, G. D. Padfield, and A. W. Gubbels, “Rotorcraft simulation fidelity: new

methods for quantification and assessment," *Aeronaut. J.*, vol. 117, no. 1189, pp. 235–282, 2013, doi: 10.1017/s0001924000007983.

[35] A. W. Gubbels, S. J. R. P. Carignan, and D. K. Ellis, "The NRC Bell 412 Advanced Systems Research Aircraft - Facility description and results of initial in-flight evaluation," *Am. Helicopter Soc. 58th Annu. Forum, Montr.*, 2002.

[36] G. D. Padfield, *Helicopter Flight Dynamics*, 2nd ed. Blackwell Publishing, 1996.

[37] M. D. White, P. Perfect, G. D. Padfield, A. W. Gubbels, and A. C. Berryman, "Acceptance testing and commissioning of a flight simulator for rotorcraft simulation fidelity research," *Proc. Inst. Mech. Eng. Part G J. Aerosp. Eng.*, vol. 227, no. 4, pp. 663–686, 2013, doi: 10.1177/0954410012439816.

[38] C. J. Ockier, "Forschungsbericht 98-07: Evaluation of the ADS-33 Handling Qualities Criteria Using the Bo 105 Helicopter," *DLR*, 1998.

[39] C. H. Kääriä, J. S. Forrest, and I. Owen, "The virtual AirDyn: A simulation technique for evaluating the aerodynamic impact of ship superstructures on helicopter operations," *Aeronaut. J.*, vol. 117, no. 1198, pp. 1233–1248, 2013, doi: 10.1017/S0001924000008836.

[40] N. A. Watson, M. F. Kelly, I. Owen, and M. D. White, "The aerodynamic effect of an oblique wind on helicopter recovery to the Queen Elizabeth class aircraft carrier," *Vert. Flight Soc. - Forum 75, Philadelphia, PN*, 2019.

[41] A. H. Roscoe and A. H. Ellis, "Technical Report TR 90019: A subjective rating scale for assessing pilot workload in flight: A decade of practical use," *R. Aerosp. Establ.*, 1990.

[42] G. E. Cooper and R. P. Harper, "NASA Tecnical Note: TN-D-5153: The use of pilot rating in the evaluation of aircraft handling qualities," Moffett Field, CA, 1969. [Online]. Available: https://ntrs.nasa.gov/archive/nasa/casi.ntrs.nasa.gov/19690013177.pdf.

[43] G. D. Padfield, J. P. Jones, M. T. Charlton, S. E. Howell, and R. Bradley, "Where Does The Workload Go When Pilots Attack Manoeuvres? An Analysis Of Results From Flying Qualities Theory And Experiment," *Twent. Eur. Rotorcr. Forum*, no. September 1994, 1994.

Appendix:

A. Bedford workload rating scale [41]:

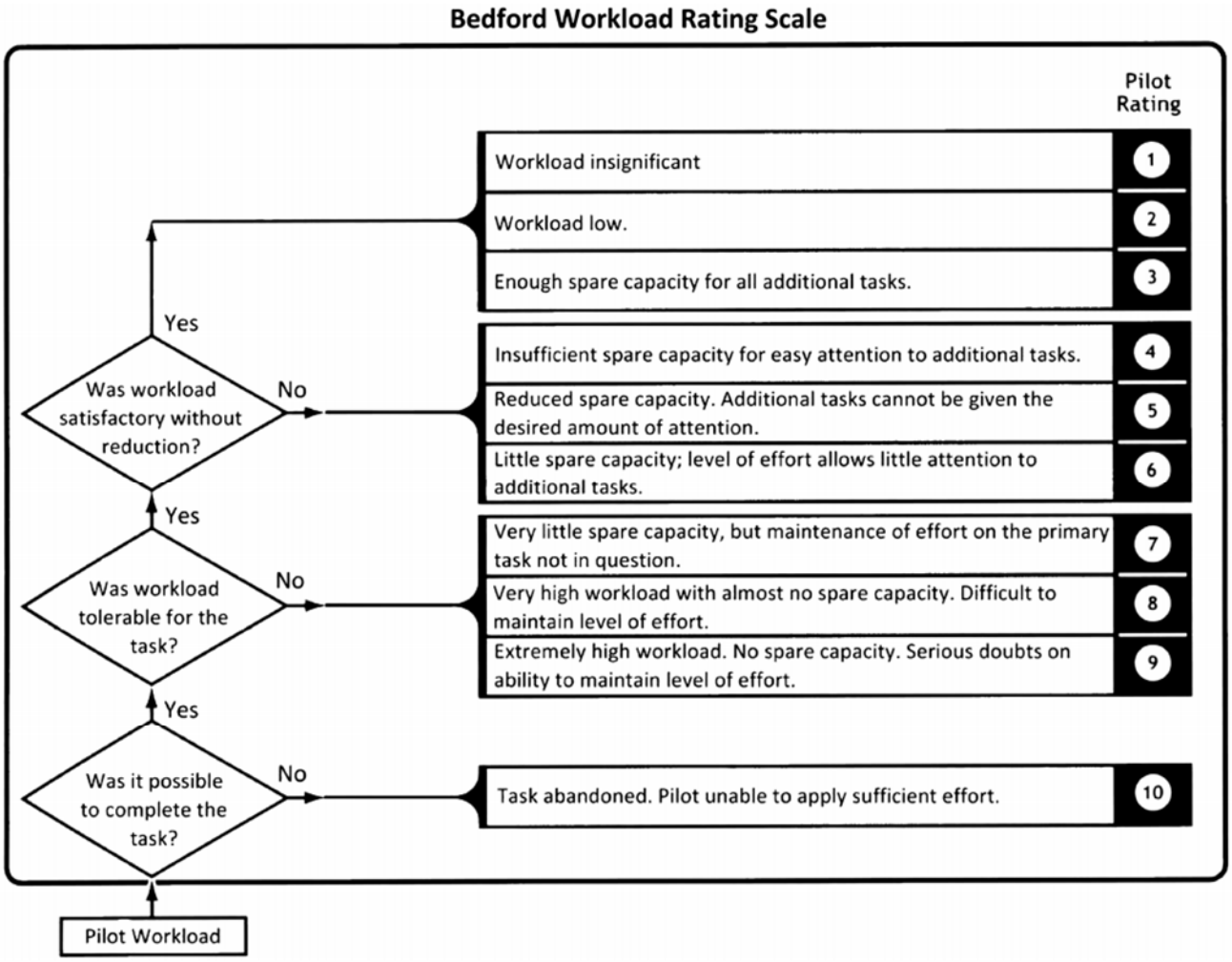

B. Cooper – Harper handling qualities rating scale [42]: